Possible correlations between gamma-ray burst and its host galaxy offset

Fei-Fei Wang [a], Yuan-Chuan Zou [a,*], Yu Liu [a], Bin Liao [a], Reetanjali Moharana [b]

[a] *School of Physics, Huazhong University of Science and Technology, Wuhan 430074, China*
[b] *Racah Institute of Physics, The Hebrew University, Jerusalem 91904, Israel*

ARTICLE INFO

ABSTRACT

We collected the information of 304 gamma-ray bursts (GRBs) from the literature, and analyzed the correlations among the host galaxy offsets (the distance from the site of the GRB to the center of its host galaxy), $T_{90,\mathrm{i}}$ (the duration T_{90} in rest-frame), $T_{R45,\mathrm{i}}$ (the duration T_{R45} in rest-frame), $E_{\gamma,\mathrm{iso}}$ (the isotropic equivalent energy), $L_{\gamma,\mathrm{iso}}$ ($= E_{\gamma,\mathrm{iso}}/T_{90,\mathrm{i}}$, the isotropic equivalent luminosity) and L_{pk} (peak luminosity). We found that $T_{90,\mathrm{i}}$, $T_{R45,\mathrm{i}}$, $E_{\gamma,\mathrm{iso}}$, L_{pk} have negative correlation with offset, which is consistent with origin of short GRBs (SGRBs) and long GRBs (LGRBs). On separate analysis, we found similar results for $\log E_{\gamma,\mathrm{iso}} - \log(\mathrm{offset})$ and $\log L_{\mathrm{pk}} - \log(\mathrm{offset})$ relations in case of SGRBs only, while no obvious relation for LGRBs. There is no correlations between offset and $L_{\gamma,\mathrm{iso}}$. We also put the special GRB 170817A and GRB 060218A on the plots. The two GRBs both have low luminosity and small offset. In the $\log(\mathrm{offset}) - \log T_{90,\mathrm{i}}$ plot, we found GRB 170817A locates in between the two regions of SGRBs and LGRBs and it is the outlier in the offset $- E_{\gamma,\mathrm{iso}}$, offset $- L_{\gamma,\mathrm{iso}}$ and offset $- L_{\mathrm{pk}}$ plots. Together with GRB 060218A being an outlier in all plots, it indicates the speciality of GRBs 170817A and 060218A, and might imply more subgroups of the GRB samples.

© 2018 Elsevier B.V. All rights reserved.

1. Introduction

Gamma-ray bursts (GRBs) are widely accepted to have two categories, short GRBs (SGRBs) having duration shorter than 2 s and long GRBs (LGRBs) with duration longer than 2 s (Kouveliotou et al., 1993). SGRBs are thought to be from the merger of compact object binaries involving at least one neutron star (Eichler et al., 1989; Paczynski, 1991; Narayan et al., 1992), and have a broad range of spatial host galaxy distribution (Zhang et al., 2017b). The origin of LGRBs are most-likely to be the collapse of rapidly-rotating massive stars (MacFadyen and Woosley, 1999), hence expected to be inside the star forming region. Consequently, the offsets of the location in the host galaxy of LGRBs are mostly smaller than those of SGRBs.

In the past few decades, there have been many studies on host galaxy offsets of GRBs. For example, Bloom et al. (2002) studied host galaxy offsets for LGRBs. The result was consistent with the expected distribution of massive stars, confirming the core-collapse model as the origin of LGRBs. Fong et al. (2010) presented the first comprehensive analysis of *Hubble Space Telescope* (*HST*) observations of ten SGRBs host galaxies. Their result showed an median

at 5 kpc for SGRBs host galaxy offsets, which is about 5 times larger than LGRBs. There was no evidence of differences between SGRBs with and without extended emission. The host galaxy offsets are in good agreement with neutron star binary mergers (see also Church et al., 2011). However, Malesani et al. (2007) noticed that SHBs (short hard GRBs) with extended emission are more easier to detect their optical counterparts. This has been explained as an environmental property by Troja et al. (2008), as SHBs with extended emission seem to occur closer to their host galaxies, in denser interstellar environments. This also implies that SGRBs progenitors have an intrinsically different behavior, due to their association with different origins such as black hole (BH)-neutron star (NS) and NS–NS merger. Troja et al. (2008) showed that SGRBs with extended hard X-ray emissions that have small projected physical offsets may be due to NS–BH mergers, while those without extended hard X-ray emission components that have bigger projected physical offsets may be due to NS–NS mergers. The correlation between X-ray absorption column densities and host galaxy offsets gives another evidence that SGRBs possibly have two distinct populations (Kopač et al., 2012). Furthermore, some negative correlations are found between the broadband afterglow emissions and SGRBs host galaxy offsets (Zhang et al., 2017b). This is because the afterglow emission depends on the circum-burst medium and it decreases with the distance to the host galaxy cen-

---

* Corresponding author.
   E-mail address: zouyc@hust.edu.cn (Y.-C. Zou).

ter, providing more evidences that SGRBs with larger host galaxy offsets prefer lower circum-burst densities (Fong et al., 2015).

To investigate the properties of the host galaxies and the connection to the GRBs, we collect all the possible sample from the literature about the offsets, durations of the GRBs (T_{90} (time duration from 5% photon counts to 95% photon counts) and T_{R45} (defined in Reichart et al., 2001)), the isotropic equivalent γ-ray energy $E_{\gamma,\mathrm{iso}}$, and the 1 s time binned peak luminosity L_{pk}. In this work we analyze these data and present our results for the relations found for SGRBs, LGRBs and combination of them. The paper is organized as the follow: the data is collected and described in §2, the statistics is performed in §3, and conclusion and discussion is given in §4.

2. The GRB sample

We selected 304 GRBs from different instruments, and collected their trigger time, instrument, redshift z, offset, T_{90}, T_{R45}, $E_{\gamma,\mathrm{iso}}$ and L_{pk} values from different published papers. All the information is provided in Table 3 and 4. $E_{\gamma,\mathrm{iso}}$ and L_{pk} are in rest-frame 1–10^4 keV energy band, and L_{pk} is in 1 s time bin (except GRB 170817A in 50 ms time bin). We also calculated isotropic equivalent luminosity $L_{\gamma,\mathrm{iso}}$ in the rest-frame 1–10^4 keV energy band, which is $L_{\gamma,\mathrm{iso}} = (1 + z)E_{\gamma,\mathrm{iso}}/T_{90}$. For L_{pk}, sometimes the energy band is not in rest-frame 1–10^4 keV energy band, like Deng et al. (2016). We changed the energy band using the spectral information. There are mainly three kinds of spectral models: Band model, cutoff power law (CPL) model and simple power law (SPL) model (more details in Li et al., 2016). In Table 4, we gave the GRB spectral information which need to change the energy band, as well as the L_{pk}. For Band model, α, β and E_{pk} are low energy spectral index, high energy spectral index and peak energy, respectively. For CPL model, α is the spectral index for the power law band and E_{pk} is the cutoff energy. There is no β for CPL model, and we use "..." to remark β. Besides, we excluded some values with lower limit smaller than 0. For example, the offset of GRB 120119A is 0.104 ± 0.147 (Li et al., 2016).

The data are not complete, as not every GRB has all the observational values listed above, available. Some of the data have only the central values available without error bars. To keep the information of the central values, we need to impute the errors from other data. We used the R package *mice* to impute the error bars for the data that have just the central values, by multiple imputation with chained equations (MICE) (Rubin, 1987, 1996).

2.1. Error imputation

We use the R package *mice* to impute incomplete multivariate data by using the method MICE. MICE is a powerful tool for imputation and it has been widely used. Only the central values with missing error bars are imputed. The ones with missing central values are omitted in the statistical analysis. According to Rubin (1987, 1996), MICE includes three steps: generating multiple imputation, analyzing imputed data, and pooling analysis results.

The imputation model should also have three principles: accounting for the process that created the missing data, preserving the relations in the data and preserving the uncertainty about these relations. At first, we changed $T_{90,i}$, $T_{R45,i}$, $E_{\gamma,\mathrm{iso}}$ and host galaxy offset into their logarithmic values. Then we did 5 times imputation as suggested in Rubin (1996). It means every error bar which need to be imputed will have 5 imputed values, hence we have 5 complete set of data. We need to choose the imputation model first, because our data is missing at random (MAR) (Rubin, 1976), additionally, our data is numeric type. So we choose the predictive mean matching model (PMM) (Little, 1988), a general

purpose semi-parametric imputation method.[1] We set a threshold at 0.25, which means the minimum proportion of usable cases for imputation is at least 0.25. An important step in multiple imputation is that, we want to assess whether imputations are plausible, then we have done diagnostic checks. We used following three indicators to assess the goodness of our imputation results.

1. Relative increase in variance due to missing data r_{m} (RIV): It is the ratio between imputation variance and the imputation variance of the 5 data sets, then multiplying the imputation time m. It stands for the increase fraction in variance due to missing data, the influence of the missing data is bigger when r_{m} is bigger. While smaller r_{m} indicates influence of the change of m is smaller, this is to say that missing data has smaller influence to the whole data parameters, hence the imputation results are more stable and the imputations are better.

$$r_m = \frac{(1 + \frac{1}{m})\sigma_{\mathrm{B}}^2}{\sigma_{\mathrm{W}}^2}. \tag{1}$$

σ_{W}^2 is within-imputation variance, it represents the mean of the variance for the m data sets.

$$\sigma_{\mathrm{W}}^2 = \frac{1}{m}\sum_{i=1}^{m}\sigma_{\mathrm{i}}^2.$$

σ_{B}^2 is between-imputation variance, it represents the variance of the mean of m data sets.

$$\sigma_{\mathrm{B}}^2 = \frac{1}{m-1}\sum_{i=1}^{m}\left(\widehat{\theta_i} - \widehat{\theta}\right)^2$$

$\widehat{\theta_i}$ is the mean of every complete data set, $\widehat{\theta} = \frac{1}{m}\sum_{i=1}^{m}\widehat{\theta_i}$.

2. Fraction of missing information γ_{m} (FMI): This represents the influence of the missing data for the whole parameters(e.g. mean). Smaller FMI values indicate that the imputation results are more stable.

$$\gamma_{\mathrm{m}} = \frac{r_{\mathrm{m}} + \frac{2}{v_{\mathrm{m}}+3}}{r_{\mathrm{m}} + 1} \tag{2}$$

$v_{\mathrm{m}} = (m-1)(1 + \frac{1}{r_{\mathrm{m}}}^2)$ is the degree of freedom.

3. Relative efficiency (RE): is a comprehensive analysis of RIV and FMI. It represents the imputation fraction for missing information by MICE. The higher value of RE means the better result.

$$\mathrm{RE} = (1 + \frac{\gamma_{\mathrm{m}}}{m})^{-1} \tag{3}$$

For analyzing imputed data and pooling analysis results, we use the mean of every imputed error bar, because we also need to calculate some values and plot scatter plots with error bars. As there are 5 candidate values for each parameter, we use the mean of them as the imputed error.

The imputation results are shown in Table 1. From the results, we can see that RIV and FMI are very close to 0, which means our

---

[1] We compared the correlations between the central values and the related errors, and found the PMM is reliable in the error imputation. For example, the positive error of $T_{90,i}$ is $T_{90,i,1}$. Before imputation, the linear regression between $T_{90,i}$ and $T_{90,i,1}$ is $T_{90,i} = (1.26 \pm 0.05) + (-9.28 \pm 1.58) \times T_{90,i,1}$, and the Pearson coefficient is -0.33 ± 0.05 with p-value 1.2×10^{-8}. After the imputation, the linear regression between $T_{90,i}$ and $T_{90,i,1}$ is $T_{90,i} = (1.27 \pm 0.05) + (-9.7 \pm 1.58) \times T_{90,i,1}$, and the Pearson coefficient is -0.33 ± 0.05 with p-value 1.6×10^{-9}. The results do not change too much, which means PMM model can preserve the relations in the data and preserve the uncertainty about these relations.

Table 1

The imputation result for some parameters' error bars. The definitions for RIV, FMI, RE are shown in section 2.1. The subscript 1 and 2 represent positive error bar and negative error bar respectively.

Parameter	RIV	FMI	RE
$T_{90,i,1}$	1.56585E−04	1.56573E−04	0.99997
$T_{90,i,2}$	6.62888E−05	6.62866E−05	0.99999
$T_{R45,i,1}$	9.40554E−05	9.40510E−05	0.99998
$T_{R45,i,2}$	8.64797E−05	8.64759E−05	0.99998
$E_{\gamma,iso,1}$	5.41595E−05	5.41581E−05	0.99999
$E_{\gamma,iso,2}$	3.75877E−05	3.75870E−05	0.99999
$offset_1$	2.43425E−02	2.40396E−02	0.99522
$offset_2$	2.84502E−03	2.84096E−03	0.99943
$L_{\gamma,iso,1}$	2.98363E−05	2.98358E−05	0.99999
$L_{\gamma,iso,2}$	3.65546E−04	3.65479E−04	0.99993

imputation is stable. RE is very close to 1, which means our imputation efficiency is very high, as per the definition. We almost imputed all the missing information. Therefore, we justify the imputation is reliable.

3. Correlation method and results

Due to the special features of GRB 170817A and GRB 060218A, we have not included them in our statistical analysis. To figure out the intrinsic connections between different properties associated with the GRBs, we convert the values into rest frame. We changed T_{90} and T_{R45} from observer-frame to rest-frame by dividing them with $1+z$ and assigned them as $T_{90,i}$ and $T_{R45,i}$ respectively. At first, we analyzed using the combined sample of both SGRBs and LGRBs. Then we separated the GRBs into SGRB group and LGRBs group, and did the same statistical analysis for the two groups separately.

In order to make sure the results are reliable, we have used several statistical analysis narrated below. At first, we calculated the correlation coefficients to check the linear correlations between different parameters, with Pearson, Spearman and Kendall τ correlation methods (Feigelson and Babu, 2012). Pearson correlation coefficient is to measure whether the two parameters are aligned in the two-dimension plot. Spearman and Kendall τ correlation coefficients are methods to measure the monotony of the two parameters. Then we did the linear regression to get the parameters of the linear expression.

For all the correlation coefficients and linear regression, we have done hypothetical tests. Once the results pass through the hypothetical tests with p-value smaller than 0.1 we accepted the correlation, as this value gives a high probability of relying the result. In the correlation statistics we have considered the error following the method used in Zou et al. (2018). Assuming the errors are normally distributed, we generated 10^3 sets of random samples with Monte Carlo (MC) simulation. Then we have done the above mentioned statistics for the 10^3 sets and checked their distribution. The best fit and corresponding 1σ errors are finally obtained.

Using above mentioned methods we found significant correlations for the following pairs, $\log(\mathrm{offset}) - \log T_{90,i}$, $\log(\mathrm{offset}) - \log T_{R45,i}$, $\log(\mathrm{offset}) - \log E_{\gamma,iso}$, $\log(\mathrm{offset}) - \log L_{pk}$, and $\log E_{\gamma,iso} - \log T_{R45,i}$. The correlation of $\log T_{90,i}$ and $\log T_{R45,i}$ is also tight. But it is trivial, and we will not discuss about it further. The $\log E_{\gamma,iso} - \log T_{90,i}$ relation is not shown here as it has been extensively investigated. All the correlation coefficient results are listed in Table 2. For the combined GRBs, the linear coefficients are significant for all the five relation pairs, the significance of correlation has further been verified with the hypothetical tests for the linear regression coefficients.

We have shown the scatter plots in Fig. 1. One can confirm the five correlations intuitively with the scatter plots. In the figures, the fitting line is in blue which was obtained by considering all the errors with MC method similar as in Zou et al. (2018). The relations obtained are as following,

$$\log(\mathrm{offset}) = -0.27^{+0.02}_{-0.02} \times \log T_{90,i} + 0.59^{+0.01}_{-0.03}, \tag{4}$$

$$\log(\mathrm{offset}) = -0.34^{+0.01}_{-0.03} \times \log T_{R45,i} + 0.4^{+0.01}_{-0.02}, \tag{5}$$

$$\log(\mathrm{offset}) = -0.14^{+0.01}_{-0.02} \times \log E_{\gamma,iso,52} + 0.38^{+0.02}_{-0.02}, \tag{6}$$

$$\log(\mathrm{offset}) = -0.11^{+0.01}_{-0.02} \times \log L_{pk,52} + 0.25^{+0.03}_{-0.03}, \tag{7}$$

$$\log E_{\gamma,iso,52} = 0.71^{+0.01}_{-0.01} \times \log T_{R45,i} + 0.36^{+0.01}_{-0.01}, \tag{8}$$

where the offset is in unit of kpc, $T_{90,i}$ and $T_{R45,i}$ are in units of seconds, $L_{pk,52}$ is in unit of 10^{52} ergs/s and $E_{\gamma,iso,52}$ is in unit of 10^{52} ergs. As expected the $T_{90,i}$ and $T_{R45,i}$ have similar correlation with the host galaxy offset with slope around -0.25. However there is no obvious separation between SGRBs and LGRBs in $T_{90,i}$, $T_{R45,i}$ and spatial offsets from plots as seen

Table 2

Linear coefficients between the four different parameters. All errors are in 1 σ confidence level. Pearson, Spearman and Kendall p-value are the mean p-value in the 1 σ range of its own coefficient.

| type	values	$\log T_{90,i}$ vs $\log$ offset	$\log T_{R45,i}$ vs $\log$ offset	$\log E_{\gamma,iso}$ vs $\log$ offset	$\log L_{\gamma,iso}$ vs $\log$ offset	$\log L_{pk}$ vs $\log$ offset	$\log T_{R45,i}$ vs $\log E_{\gamma,iso}$
All GRBs	Pearson coefficient	$-0.37^{+0.02}_{-0.04}$	$-0.4^{+0.02}_{-0.04}$	$-0.29^{+0.02}_{-0.04}$	$-0.03^{+0.01}_{-0.03}$	$-0.18^{+0.02}_{-0.04}$	$0.425^{+0.003}_{-0.007}$
	Pearson p-value	3.9E−05	2.8E−05	2.1E−03	0.73	0.07	3.6E−14
	Spearman coefficient	$-0.25^{+0.01}_{-0.03}$	$-0.27^{+0.01}_{-0.03}$	$-0.2^{+0.01}_{-0.03}$	$-0.03^{+0.01}_{-0.03}$	$-0.11^{+0.01}_{-0.04}$	$0.359^{+0.003}_{-0.008}$
	Spearman p-value	7.3E−03	4.1E−03	3E−02	0.74	0.25	2.9E−10
	Kendall coefficient	$-0.16^{+0.01}_{-0.02}$	$-0.18^{+0.01}_{-0.02}$	$-0.13^{+0.01}_{-0.02}$	$-0.02^{+0.01}_{-0.02}$	$-0.08^{+0.01}_{-0.03}$	$0.249^{+0.002}_{-0.005}$
	Kendall p-value	1.1E−02	6E−03	3.7E−02	0.72	0.22	2.6E−10
Short GRBs	Pearson coefficient	$-0.25^{+0.03}_{-0.07}$	$-0.35^{+0.03}_{-0.08}$	$-0.36^{+0.04}_{-0.08}$	$0.07^{+0.07}_{-0.04}$	$-0.62^{+0.03}_{-0.06}$	$0.53^{+0.01}_{-0.04}$
	Pearson p-value	0.22	0.12	0.09	0.19	0.02	0.01
	Spearman coefficient	$-0.22^{+0.03}_{-0.07}$	$-0.34^{+0.04}_{-0.07}$	$-0.37^{+0.03}_{-0.08}$	$0.07^{+0.43}_{-0.03}$	$-0.55^{+0.03}_{-0.08}$	$0.37^{+0.02}_{-0.04}$
	Spearman p-value	0.28	0.13	0.08	0.15	0.05	0.1
	Kendall coefficient	$-0.14^{+0.02}_{-0.05}$	$-0.22^{+0.03}_{-0.06}$	$-0.27^{+0.03}_{-0.06}$	$0.06^{+0.45}_{-0.03}$	$-0.42^{+0.03}_{-0.06}$	$0.25^{+0.02}_{-0.03}$
	Kendall p-value	0.3	0.16	0.07	0.14	0.05	0.11
Long GRBs	Pearson coefficient	$0.1^{+0.02}_{-0.05}$	$0.08^{+0.02}_{-0.04}$	$0.05^{+0.01}_{-0.04}$	$0.02^{+0.01}_{-0.04}$	$0.09^{+0.02}_{-0.04}$	$0.196^{+0.004}_{-0.01}$
	Pearson p-value	0.43	0.54	0.69	0.88	0.47	1.4E−03
	Spearman coefficient	$0.12^{+0.02}_{-0.04}$	$0.07^{+0.02}_{-0.04}$	$0.07^{+0.01}_{-0.04}$	$0.03^{+0.02}_{-0.04}$	$0.07^{+0.02}_{-0.04}$	$0.237^{+0.004}_{-0.009}$
	Spearman p-value	0.32	0.56	0.57	0.86	0.59	9.8E−05
	Kendall coefficient	$0.09^{+0.01}_{-0.03}$	$0.06^{+0.01}_{-0.03}$	$0.05^{+0.01}_{-0.03}$	$0.02^{+0.01}_{-0.03}$	$0.05^{+0.01}_{-0.03}$	$0.16^{+0.003}_{-0.007}$
	Kendall p-value	0.27	0.5	0.54	0.86	0.62	1E−04
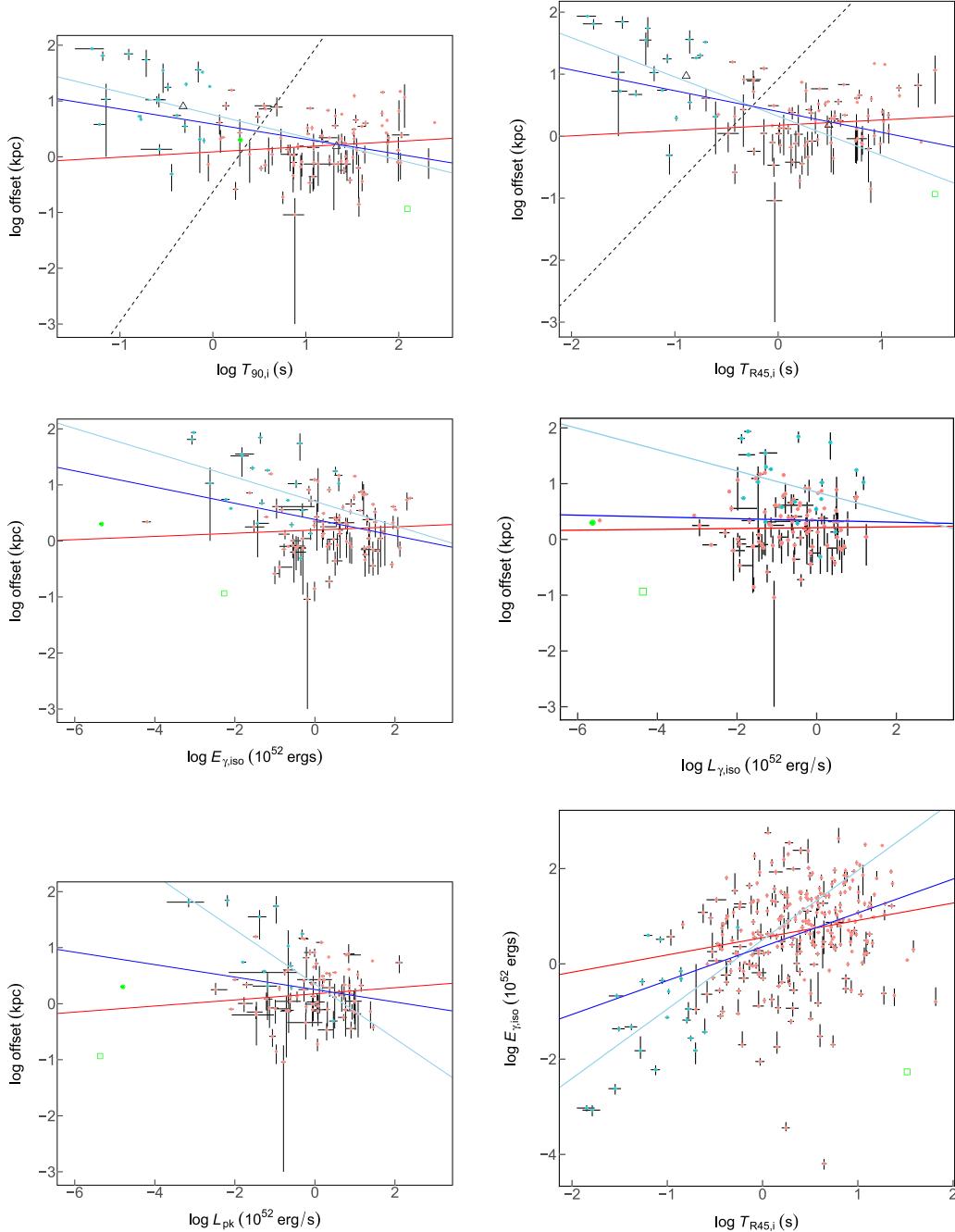
Fig. 1. The scatter plots and linear regression results between two different parameters, offset$-T_{90,i}$, offset$-T_{R45,i}$, offset$-E_{\gamma,iso}$, offset$-L_{\gamma,iso}$, offset$-L_{pk}$ and $E_{\gamma,iso}-T_{R45,i}$ respectively, which are all shown in logarithmic scale. The red points are for LGRBs, and the sky blue points are for SGRBs. The red line is the linear regression result for LGRBs. The sky blue line is the linear regression result for SGRBs. The blue line is the linear regression result for all GRBs. The black dashed line is the result for k-means classification. The two black triangles are the cluster centers. The green circle point is GRB 170817A in offset$-T_{90,i}$, offset$-L_{\gamma,iso}$, offset$-L_{pk}$ and offset$-E_{\gamma,iso}$ plots. The green square point is GRB 060218A in all plots. All the linear regression results are derived with MC method similar as in Zou et al. (2018). (For interpretation of the colors in the figure(s), the reader is referred to the web version of this article.)

in Troja et al. (2008) for T_{90} and spatial offset scatter plot. We assume this discrepancy is due to the redshift correction. Interestingly, in the log (offset) $-\log T_{90,i}$ plot, there are four LGRBs with $T_{90,i} < 2$, and there is a gap between these short ones and the normal LGRBs. This might indicate that the separation of LGRBs and SGRBs should be in the rest frame rather than the observer's frame. The anti-correlation between offset and the duration is consistent with the double degenerated star merger origin for SGRBs and massive star core-collapsing origin for LGRBs. For mergers, they have to pass supernova explosion, which kicks the central compact star. And it takes time for the double compact star to merge, which lead the site of the merging to be in the outer part of the

host galaxy. While for the massive star core-collapsing, it should be in the star forming region, which is near the center of the host galaxy.

The anti-correlation between offset and $E_{\gamma,iso}$, L_{pk} respectively may also be related to the LGRBs and SGRBs, as LGRBs are relatively stronger in γ-rays, which can also be seen in the log $E_{\gamma,iso} -$ log $T_{R45,i}$ scattering plot. However we could not find an exact explanation for the values of the slopes and intercepts. We assume a detail analysis of the star forming and merger profile in the galaxies would be able to explain these parameters, however this analysis is beyond the scope of our paper.

Table 3

Sample for the quantities related to the offset of the GRB host galaxies. The definition of each parameter is shown in Section 2.

GRB	Time	Instrument	z	T_{90} (s)	T_{R45} (s)	$E_{\gamma,iso}$ (10^{52} ergs)	offset (kpc)	ref
170817A	12:41:06.47	Fermi	0.00968	$2.0^{+0.5}_{-0.5}$	...	$4.7E-6^{+7E-7}_{-7E-7}$	$2.0^{+0.2}_{-0.2}$	(1);(2);(1);(3)
130907A	21:41:13	Swift/KW	1.238	357^{+2}_{-2}	$40.31^{+0.14}_{-0.14}$	304^{+19}_{-19}	...	(4);(5);(5);(4)
130831A	13:04:16	Swift/KW	0.4791	$34.65^{+0.53}_{-0.53}$	$4.07^{+0.02}_{-0.02}$	$0.46^{+0.02}_{-0.02}$	...	(4);(5);(5);(4)
130701A	04:17:43	Swift/KW	1.155	$4.62^{+0.09}_{-0.09}$	$1.62^{+0.03}_{-0.03}$	$2.60^{+0.09}_{-0.09}$	...	(4);(5);(5);(4)
130610A	03:12:13	Swift/Fermi	2.092	$48.5^{+2.4}_{-2.4}$	$9.3^{+0.3}_{-0.3}$	$6.99^{+0.46}_{-0.46}$	...	(4);(5);(5);(4)
130606A	21:04:39	Swift/KW	5.91	$278.5^{+3.5}_{-3.5}$	$11.77^{+0.68}_{-0.68}$	$28.3^{+5.1}_{-5.1}$	$0.36^{+0.12}_{-0.12}$	(4);(5);(5);(4);(6)
130603B	15:49:14	Swift/KW	0.356	$0.22^{+0.01}_{-0.01}$	$0.040^{+0.007}_{-0.007}$	$0.212^{+0.023}_{-0.023}$	$5.3^{+0.2}_{-0.2}$	(7);(5);(5);(4);(6)
130528A	16:41:23	Swift/Fermi	1.25	652^{+17}_{-17}	$19.22^{+0.93}_{-0.93}$	$4.48^{+0.41\,c}_{-0.38}$	...	(8);(5);(5);(9)
130514A	07:13:41	Swift	3.6	$220.3^{+5.6}_{-5.6}$	$34.02^{+0.87}_{-0.87}$	$52.4^{+9.2}_{-9.2}$	...	(4);(5);(5);(4)
130505A	08:22:28	KW/Swift	2.27	293^{+34}_{-34}	$6.23^{+0.62}_{-0.62}$	347^{+35}_{-35}	...	(4);(5);(5);(4)
130427B	13:20:41	Swift	2.78	$7.04^{+0.26}_{-0.26}$	$2.2^{+0.1}_{-0.1}$	$5.04^{+0.48}_{-0.48}$	...	(4);(5);(5);(4)
130427A	07:47:57	Swift/Fermi	0.334	$324.7^{+2.5}_{-2.5}$	$7.64^{+0.38}_{-0.38}$	92^{+13}_{-13}	$4.1^{+0.1}_{-0.1}$	(4);(5);(5);(4);(6)
130420A	07:28:29	Swift/Fermi	1.297	$114.8^{+4.8}_{-4.8}$	$21.56^{+0.46}_{-0.46}$	$7.74^{+0.77}_{-0.77}$	...	(4);(5);(5);(4)
130215A	01:31:30	Swift/Fermi	0.597	$89.1^{+8.4}_{-8.4}$	$19.5^{+1.2}_{-1.2}$	$3.1^{+1.6}_{-1.6}$	...	(10);(5);(5);(11)
121217A	07:17:47	Swift/Fermi	3.1	848^{+12}_{-12}	$64.8^{+2.0}_{-2.0}$	62^{a}	...	(12);(5);(5);(12)
121211A	13:47:02	Swift/Fermi	1.023	$184.1^{+2.3}_{-2.3}$	$15.2^{+1.5}_{-1.5}$	$0.49^{+0.1}_{-0.1}$	...	(13);(5);(5);(13)
121201A	12:25:42	Swift	3.385	$39.0^{+2.9}_{-2.9}$	$8.96^{+0.53}_{-0.53}$	$2.52^{+0.34}_{-0.34}$	...	(4);(5);(5);(4)
121128A	05:05:37	Swift/Fermi	2.2	$25.7^{+5.5}_{-5.5}$	$4.8^{+0.2}_{-0.2}$	$8.66^{+0.87}_{-0.87}$	...	(4);(5);(5);(4)
121027A	07:32:29	Swift	1.773	$69.3^{+1.9}_{-1.9}$	$15.00^{+0.57}_{-0.57}$	$3.29^{+0.17}_{-0.17}$	...	(4);(5);(5);(4)
121024A	02:56:12	Swift	2.298	$12.46^{+0.39}_{-0.39}$	$2.94^{+0.19}_{-0.19}$	$4.61^{+0.55}_{-0.55}$	...	(4);(5);(5);(4)
120909A	01:42:03	Swift/Fermi	3.93	618^{+31}_{-31}	$45.0^{+2.4}_{-2.4}$	87^{+10}_{-10}	...	(4);(5);(5);(4)
120907A	00:24:23	Swift/Fermi	0.97	$6.27^{+0.28}_{-0.28}$	$1.11^{+0.07}_{-0.07}$	$0.27^{+0.04}_{-0.04}$	...	(13);(5);(5);(13)
120815A	02:13:58	Swift	2.358	$9.7^{+1.2}_{-1.2}$	$1.76^{+0.15}_{-0.15}$	$1.65^{+0.27}_{-0.27}$	...	(4);(5);(5);(4)
120811C	15:34:52	Swift/Fermi	2.671	$25.2^{+1.3}_{-1.3}$	$6.15^{+0.13}_{-0.13}$	$6.41^{+0.64}_{-0.64}$	...	(4);(5);(5);(4)
120804AS	00:54:14	Swift	$1.3^{+0.3}_{-0.2}$	$1.78^{+0.32}_{-0.32}$	$0.32^{+0.02}_{-0.02}$	$0.70^{+0.15}_{-0.15}$	...	(14);(5);(5);(4)
120802A	08:00:51	Swift	3.796	$50.2^{+1.5}_{-1.5}$	$5.4^{+0.22}_{-0.22}$	$12.9^{+2.8}_{-2.8}$	...	(4);(5);(5);(4)
120729A	10:56:14	Swift/Fermi	0.8	$78.7^{+6.5}_{-6.5}$	$7.70^{+0.29}_{-0.29}$	$2.3^{+1.5}_{-1.5}$	...	(15);(5);(5);(11)
120712A	13:42:27	Swift/Fermi	4.175	$18.5^{+1.1}_{-1.1}$	$4.68^{+0.15}_{-0.15}$	$21.2^{+2.1}_{-2.1}$	...	(4);(5);(5);(4)
120624B	22:23:54.9339	Fermi	2.197	$174.72^{+0.28}_{-0.28}$	$38.2^{+0.3}_{-0.3}$	319^{+32}_{-32}	...	(4);(5);(5);(4)
120521C	23:22:07	Swift	6	$33.2^{+2.4}_{-2.4}$	$5.32^{+0.24}_{-0.24}$	19^{+8}_{-8}	...	(15);(5);(5);(16)
120404A	12:51:02	Swift	2.876	$40.5^{+1.5}_{-1.5}$	$12.15^{+0.46}_{-0.46}$	$4.18^{+0.34}_{-0.34}$	...	(4);(5);(5);(4)
120327A	02:55:16	Swift	2.813	$71.2^{+2.3}_{-2.3}$	$10.20^{+0.33}_{-0.33}$	$14.42^{+0.46}_{-0.46}$	...	(4);(5);(5);(4)
120326A	01:20:29	Swift/Fermi	1.798	$72.7^{+3.1}_{-3.1}$	$4.68^{+0.11}_{-0.11}$	$3.27^{+0.33}_{-0.33}$	...	(4);(5);(5);(4)
120119A	04:04:30.21	Swift/Fermi	1.728	$70.4^{+4.3}_{-4.3}$	$13.6^{+0.2}_{-0.2}$	$27.2^{+3.6}_{-3.6}$	...	(4);(5);(5);(4)
111228A	15:44:43	Swift/Fermi	0.716	$101.4^{+1.3}_{-1.3}$	$9.00^{+0.31}_{-0.31}$	$2.75^{+0.28}_{-0.28}$	...	(4);(5);(5);(4)
111117AS	12:13:41	Swift/Fermi	$1.31^{+0.46}_{-0.23}$	$0.58^{+0.14}_{-0.14}$	...	$0.34^{+0.13}_{-0.13}$	$10.5^{+1.7}_{-1.7}$	(14);(17);(4);(18)
111107A	00:50:24	Swift/Fermi	2.893	$31.6^{+2.4}_{-2.4}$	$5.46^{+0.29}_{-0.29}$	$3.76^{+0.55}_{-0.55}$	...	(4);(5);(5);(4)
111008A	22:12:58	Swift/KW	4.9898	$75.7^{+2.3}_{-2.3}$	$10.92^{+0.54}_{-0.54}$	$24.7^{+1.2}_{-1.2}$	...	(4);(5);(5);(4)
110818A	20:37:49	Swift/Fermi	3.36	$77.3^{+5.6}_{-5.6}$	$20.16^{+0.83}_{-0.83}$	$26.6^{+2.8}_{-2.8}$	...	(4);(5);(5);(4)
110801A	19:49:42	Swift/KW	1.858	400^{+2}_{-2}	$54.6^{+1.7}_{-1.7}$	$10.9^{+2.7}_{-2.7}$	...	(4);(5);(5);(4)
110731A	11:09:30	Swift/Fermi	2.83	$46.6^{+7.1}_{-7.1}$	$3.360^{+0.071}_{-0.071}$	$49.5^{+4.9}_{-4.9}$	$1.47^{+0.08}_{-0.08}$	(4);(5);(5);(4);(6)
110715A	13:13:50	Swift/KW	0.82	$13.2^{+1.4}_{-1.4}$	$1.450^{+0.025}_{-0.025}$	$4.36^{+0.45}_{-0.45}$	...	(4);(5);(5);(4)
110503A	17:35:45	Swift/KW	1.613	$9.31^{+0.64}_{-0.64}$	$2.100^{+0.056}_{-0.056}$	$20.8^{+2.1}_{-2.1}$	...	(4);(5);(5);(4)
110422A	15:41:55	Swift/KW	1.77	$26.73^{+0.29}_{-0.29}$	$9.24^{+0.09}_{-0.09}$	$79.8^{+8.2}_{-8.2}$	...	(4);(5);(5);(4)
110213A	05:17:29	Swift/Fermi	1.46	$43.1^{+3.5}_{-3.5}$	$6.44^{+0.32}_{-0.32}$	$5.78^{+0.81}_{-0.81}$	...	(4);(5);(5);(4)
110205A	02:02:41	Swift/KW	2.22	$277^{+4.7}_{-4.7}$	$74.52^{+0.91}_{-0.91}$	$48.3^{+6.4}_{-6.4}$	...	(4);(5);(5);(4)
110106B	21:26:17	Swift/Fermi	0.618	27^{+1}_{-1}	$8.12^{+0.31}_{-0.31}$	$0.73^{+0.07}_{-0.07}$	...	(4);(5);(5);(4)
101219A	02:31:29	Swift/KW	0.718	$0.86^{+0.06}_{-0.06}$	$0.240^{+0.011}_{-0.011}$	$0.488^{+0.068}_{-0.068}$	3.5^{a}	(7);(5);(5);(4);(19)
101213A	10:49:20.7987	Fermi	0.414	$175.7^{+15.3}_{-15.3}$	$20.2^{+0.7}_{-0.7}$	$2.72^{+0.53}_{-0.53}$	...	(4);(5);(5);(4)
100906A	13:49:27	Swift/Fermi	1.727	$116.85^{+0.69}_{-0.69}$	$11.07^{+0.12}_{-0.12}$	$29.9^{+2.9}_{-2.9}$	...	(4);(5);(5);(4)
100901A	13:34:10	Swift	1.408	459^{+11}_{-11}	$32.0^{+2.2}_{-2.2}$	$4.2^{+0.5}_{-0.5}$	...	(4);(5);(5);(4)
100816A	00:37:51	Swift/Fermi	0.8049	$2.50^{+0.22}_{-0.22}$	$0.840^{+0.016}_{-0.016}$	$0.71^{+0.09}_{-0.09}$	$8.2^{+1.4\,b}_{-1.4}$	(4);(5);(5);(4);(20)
100814A	03:50:11	Swift/Fermi	1.44	$177.0^{+3.6}_{-3.6}$	$31.60^{+0.75}_{-0.75}$	$15.3^{+1.8}_{-1.8}$	...	(4);(5);(5);(4)
100728B	10:31:55	Swift/Fermi	2.106	$11.52^{+0.78}_{-0.78}$	$2.56^{+0.14}_{-0.14}$	$3.55^{+0.36}_{-0.36}$	...	(4);(5);(5);(4)
100728A	02:18:24	Swift/Fermi	1.567	$222.0^{+6.9}_{-6.9}$	$57.35^{+0.19}_{-0.19}$	$86.8^{+8.7}_{-8.7}$	...	(4);(5);(5);(4)
100704A	03:35:08	Swift/Fermi	3.6	$194.6^{+4.1}_{-4.1}$	$17.44^{+0.65}_{-0.65}$	$19.1^{+6.1}_{-6.1}$	...	(10);(5);(5);(21)
100625A	18:32:28	Swift/Fermi	$0.40^{+0.06}_{-0.06}$	$0.19^{+0.14}_{-0.14}$	$0.140^{+0.007}_{-0.007}$	$0.075^{+0.003}_{-0.003}$	...	(14);(5);(5);(4)
100621A	03:03:32	Swift/KW	0.542	$66.3^{+1.3}_{-1.3}$	$19.43^{+0.33}_{-0.33}$	$2.82^{+0.35}_{-0.35}$	...	(4);(5);(5);(4)
100513A	02:07:08	Swift	4.8	$65.1^{+4.4}_{-4.4}$	19^{+1}_{-1}	$6.75^{+0.53}_{-0.53}$	...	(4);(5);(5);(4)
100413A	17:33:28	Swift/Fermi	3.9	$197.4^{+2.3}_{-2.3}$	$55.5^{+1.2}_{-1.2}$	73^{+46}_{-46}	...	(10);(5);(5);(21)
100117A	21:06:19	Swift/Fermi	0.915	$0.51^{+0.19}_{-0.19}$	...	$0.78^{+0.10}_{-0.10}$	$1.36^{+0.32}_{-0.32}$	(4);(22);(4);(6)
091208B	09:49:57	Swift/Fermi	1.063	$15.2^{+1.3}_{-1.3}$	$1.82^{+0.12}_{-0.12}$	$2.06^{+0.21}_{-0.21}$	0.79^{a}	(4);(5);(5);(4);(23)
091127A	23:25:45	Swift/Fermi	0.49	$9.57^{+0.56}_{-0.56}$	$1.540^{+0.063}_{-0.063}$	$1.64^{+0.18}_{-0.18}$	$1.35^{+0.30}_{-0.30}$	(4);(5);(5);(4);(6)

Table 3 (*continued*)

GRB	Time	Instrument	z	T_{90} (s)	T_{R45} (s)	$E_{\gamma,\mathrm{iso}}$ (10^{52} ergs)	offset (kpc)	ref
091029A	03:53:22	Swift	2.752	$40.0^{+1.3}_{-1.3}$	$11.47^{+0.23}_{-0.23}$	$7.97^{+0.82}_{-0.82}$	...	(4);(5);(5);(4)
091024A	08:56:01	Swift/Fermi	1.092	115^{+5}_{-5}	$24.64^{+0.87}_{-0.87}$	$18.4^{+2.0}_{-2.0}$	...	(4);(5);(5);(4)
091020A	21:36:44	Swift/Fermi	1.71	$39.0^{+1.1}_{-1.1}$	$6.00^{+0.17}_{-0.17}$	$8.4^{+1.1}_{-1.1}$	...	(4);(5);(5);(4)
091018A	20:48:19	Swift/Konus-RF	0.97	$4.44^{+0.15}_{-0.15}$	$1.240^{+0.022}_{-0.022}$	$0.7^{+0.3}_{-0.1}$	...	(15);(5);(5);(24)
090927	10:07:16	Swift/Fermi	1.37	$18.4^{+1.3}_{-1.3}$	$0.84^{+0.09}_{-0.09}$	$0.276^{+0.035}_{-0.035}$	...	(4);(5);(5);(4)
090926B	21:55:48	Swift/Fermi	1.24	$126.4^{+5.2}_{-5.2}$	$21.60^{+0.62}_{-0.62}$	$4.14^{+0.45}_{-0.45}$	...	(4);(5);(5);(4)
090812A	06:02:21.89	Swift/KW	2.452	100^{+16}_{-16}b	$18.50^{+0.42}_{-0.42}$b	$47.5^{+8.2}_{-8.2}$	...	(4);(25);(25);(4)
090809A	17:31:27.50	Swift	2.737	190^{+18}_{-18}b	$3.40^{+0.42}_{-0.42}$b	$1.88^{+0.26}_{-0.26}$	...	(4);(25);(25);(4)
090726	22:42:40.75	Swift	2.71	$51.00^{+0.61}_{-0.61}$b	$9.20^{+0.54}_{-0.54}$b	$1.80^{+1.3}_{-0.24}$ b	...	(24);(25);(25);(25)
090715B	21:03:27.63	Swift/KW	3	$268.0^{+4.2}_{-4.2}$b	$15.30^{+0.61}_{-0.61}$b	$23.8^{+3.7}_{-3.7}$	...	(4);(25);(25);(4)
090709A	07:38:47.59	Swift/AGILE/KW	1.8	300^{+64}_{-64}	$28.50^{+0.48}_{-0.48}$b	$20.9^{+3.6}_{-2.5}$	$2.46^{+0.31}_{-0.31}$	(26);(25);(25);(27);(6)
090618	08:28:42.85	Swift/Fermi/AGILE	0.54	$115.20^{+0.42}_{-0.42}$b	$23.00^{+0.61}_{-0.61}$b	$28.6^{+2.9}_{-2.9}$	$4.5^{+0.3}_{-0.3}$	(4);(25);(25);(4);(6)
090530	03:18:31.38	Swift	1.266	$41.00^{+0.61}_{-0.61}$b	$2.60^{+0.18}_{-0.18}$b	$1.73^{+0.19}_{-0.19}$	...	(4);(25);(25);(4)
090529	14:12:48.21	Swift	2.625	80^{+3}_{-3}b	$19.0^{+1.2}_{-1.2}$	$2.56^{+0.30}_{-0.30}$	...	(4);(25);(25);(4)
090519A	21:09:09.42	Swift/Fermi	3.85	$82.0^{+5.4}_{-5.4}$b	$14.00^{+0.61}_{-0.61}$b	$24.7^{+2.8}_{-2.8}$	...	(4);(25);(25);(4)
090516A	08:28:03.77	Swift/Fermi	4.109	$230.0^{+9.1}_{-9.1}$b	$37.0^{+1.8}_{-1.8}$	72^{+14}_{-14}	...	(4);(25);(25);(4)
090515	04:45:22.52	Swift	0.403	$0.070^{+0.024}_{-0.024}$	$0.0200^{+0.0042}_{-0.0042}$	$0.00094^{+0.00014}_{-0.00014}$	$86.2^{+0.1}_{-0.1}$	(4);(25);(25);(4);(6)
090510A	00:23:13.48	Swift/Fermi/AGILE	0.903	$0.500^{+0.061}_{-0.061}$b	$0.120^{+0.012}_{-0.012}$b	$3.95^{+0.21}_{-0.21}$	$10.6^{+2.9}_{-2.9}$	(7);(25);(25);(4);(6)
090429B	05:30:16.36	Swift	9.3	$5.8^{+0.3}_{-0.3}$	$1.50^{+0.06}_{-0.06}$	$6.7^{+1.3}_{-1.3}$	...	(4);(25);(25);(4)
090426	12:49:00.21	Swift	2.609	$1.300^{+0.061}_{-0.061}$b	$0.320^{+0.024}_{-0.024}$b	$0.445^{+0.066}_{-0.066}$	$0.49^{+0.25}_{-0.25}$	(7);(25);(25);(4);(6)
090424A	14:12:22.33	Swift/Fermi/AGILE	0.544	$50.30^{+0.54}_{-0.54}$	$1.98^{+0.03}_{-0.03}$b	$4.07^{+0.41}_{-0.41}$	$2.62^{+0.24}_{-0.24}$	(4);(25);(25);(4);(6)
090423A	07:55:32.34	Swift/Fermi	8.1	$12.40^{+0.61}_{-0.61}$b	$3.80^{+0.12}_{-0.12}$b	$8.8^{+2.1}_{-2.1}$	...	(4);(25);(25);(4)
090418A	11:07:53.22	Swift/KW	1.608	$57.97^{+0.85}_{-0.85}$	$17.05^{+0.41}_{-0.41}$	$17.2^{+2.7}_{-2.7}$	0.74a	(4);(5);(5);(4);(23)
090417B	15:20:16.33	Swift	0.34	$252.0^{+4.8}_{-4.8}$b	88^{+3}_{-3}b	$0.16^{+0.16}_{-0.03}$	...	(15);(25);(25);(28)
090404	15:56:43.44	Swift	$3.0^{+0.8}_{-1.8}$	$86.0^{+3.6}_{-3.6}$b	$21.00^{+0.61}_{-0.61}$	$5.9^{+1.8}_{-2.3}$	...	(29);(25);(25);(27)
090313A	09:06:40.42	Swift	3.375	$90.0^{+6.7}_{-6.7}$b	$23.0^{+1.2}_{-1.2}$b	$4.42^{+0.79}_{-0.79}$	...	(4);(25);(25);(4)
090205A	23:03:27.82	Swift	4.6497	$11.00^{+0.61}_{-0.61}$b	$2.60^{+0.18}_{-0.18}$	$1.12^{+0.16}_{-0.16}$	$2.7^{+2.0}_{-2.0}$	(4);(25);(25);(4);(6)
090102A	02:55:45.86	Swift/Fermi/AGILE	1.547	$31.00^{+0.61}_{-0.61}$b	$8.3^{+0.3}_{-0.3}$b	$22.6^{+2.7}_{-2.7}$	$0.78^{+0.52}_{-0.52}$	(4);(25);(25);(4);(6)
081228	01:17:40.75	Swift	3.4	$3.80^{+0.42}_{-0.42}$b	$0.480^{+0.048}_{-0.048}$b	$3.7^{+1.6}_{-1.3}$	...	(15);(25);(25);(27)
081222A	04:53:59.97	Swift/Fermi/AGILE	2.77	$33.0^{+1.2}_{-1.2}$	$4.200^{+0.054}_{-0.054}$b	$27.4^{+2.7}_{-2.7}$	...	(4);(25);(25);(4)
081221A	16:21:11.84	Swift/Fermi	2.26	$34.00^{+0.61}_{-0.61}$b	$8.00^{+0.06}_{-0.06}$b	$31.9^{+3.2}_{-3.2}$	$3.3^{+0.6}_{-0.6}$	(4);(25);(25);(4);(6)
081203A	13:57:11.57	Swift/AGILE/KW	2.05	250^{+27}_{-27}b	$31.00^{+0.61}_{-0.61}$	32^{+12}_{-12}	...	(4);(25);(25);(4)
081121A	20:35:32.85	Swift/Feimi/AGILE	2.512	$19.00^{+0.61}_{-0.61}$b	$5.50^{+0.24}_{-0.24}$b	$32.4^{+3.7}_{-3.7}$	2^{+1}_{-1}	(4);(25);(25);(4);(6)
081118	14:56:36.73	Swift	2.58	$67.0^{+4.8}_{-4.8}$	$18.00^{+0.61}_{-0.61}$b	$12.2^{+1.2}_{-1.2}$	...	(4);(25);(25);(4)
081109A	07:02:06.61	Swift/Fermi	0.9787	$70.0^{+1.8}_{-1.8}$b	$17.20^{+0.42}_{-0.42}$b	$1.81^{+0.12}_{-0.12}$	...	(4);(25);(25);(4)
081029	01:43:56.78	Swift	3.8479	$170.0^{+8.5}_{-8.5}$b	$49.0^{+2.4}_{-2.4}$b	$12.1^{+1.4}_{-1.4}$	...	(4);(25);(25);(4)
081028A	00:25:00.79	Swift	3.038	$280.0^{+9.1}_{-9.1}$b	$78.0^{+1.8}_{-1.8}$	$18.3^{+1.8}_{-1.8}$	...	(4);(25);(25);(4)
081008A	19:58:09.38	Swift/Fermi	1.969	200^{+11}_{-11}b	$32.00^{+0.61}_{-0.61}$b	10^{+1}_{-1}	$14.3^{+0.2}_{-0.2}$	(4);(25);(25);(4);(6)
081007A	05:23:52.74	Swift/Fermi	0.5295	$5.60^{+0.24}_{-0.24}$	$1.600^{+0.061}_{-0.061}$b	$0.17^{+0.02}_{-0.02}$	$0.71^{+0.18}_{-0.18}$	(4);(25);(25);(4);(6)
080928	15:01:32.86	Swift/Fermi	1.692	280^{+11}_{-11}b	$23.00^{+0.61}_{-0.61}$b	$3.99^{+0.91}_{-0.91}$	$14.8^{+0.3}_{-0.3}$	(4);(25);(25);(4);(6)
080916B	14:44:47.32	Swift	4.35	$34.0^{+1.8}_{-1.8}$b	$6.10^{+0.48}_{-0.48}$	563a	...	(30);(25);(25);(30)
080916A	09:45:20.61	Swift/Fermi	0.689	63^{+3}_{-3}b	$13.30^{+0.24}_{-0.24}$b	$1.0^{+0.1}_{-0.1}$	0.14a	(4);(25);(25);(4);(23)
080913A	06:46:54.12	Swift/KW	6.695	$8.20^{+0.24}_{-0.24}$b	$2.20^{+0.12}_{-0.12}$b	$9.2^{+2.7}_{-2.7}$	...	(4);(25);(25);(4)
080905B	16:55:45.40	Swift/Fermi	2.3739	$104.0^{+4.2}_{-4.2}$b	$13.00^{+0.61}_{-0.61}$b	$4.55^{+0.37}_{-0.37}$	...	(4);(25);(25);(4)
080905A	11:58:54.97	Swift/Fermi/AGILE	0.122	$1.04^{+0.03}_{-0.03}$b	$0.180^{+0.018}_{-0.018}$b	$0.0658^{+0.0096}_{-0.0096}$	$18.2^{+0.2}_{-0.2}$	(4);(25);(25);(4);(6)
080810A	13:10:12.28	Swift/Fermi	3.35	$453.0^{+4.8}_{-4.8}$b	$31.0^{+1.2}_{-1.2}$b	$47.8^{+5.5}_{-5.5}$	...	(4);(25);(25);(4)
080805A	07:41:34.73	Swift	1.5042	$110^{+8.5}_{-8.5}$b	$20.00^{+0.61}_{-0.61}$b	$5.05^{+0.22}_{-0.22}$	$4.0^{+0.4}_{-0.4}$	(4);(25);(25);(4);(6)
080804A	23:20:14.66	Swift/Fermi	2.205	$60.0^{+8.5}_{-8.5}$b	$7.90^{+0.36}_{-0.36}$b	$12.0^{+1.2}_{-1.2}$	...	(4);(25);(25);(4)
080721A	10:25:16.97	Swift/AGILE/KW	2.591	$30.0^{+1.8}_{-1.8}$b	$4.50^{+0.18}_{-0.18}$b	134^{+23}_{-23}	...	(4);(25);(25);(4)
080710	07:13:10.79	Swift	0.8454	$140.0^{+9.7}_{-9.7}$b	$23.0^{+1.8}_{-1.8}$b	$1.68^{+0.22}_{-0.22}$	...	(4);(25);(25);(4)
080707A	08:27:53.68	Swift	1.23	$30.30^{+0.42}_{-0.42}$b	$3.30^{+0.18}_{-0.18}$b	$0.34^{+0.25}_{-0.03}$b	$0.76^{+0.46}_{-0.46}$	(25);(25);(25);(25);(6)
080607A	06:07:27.00	Swift/AGILE/KW	3.036	$84.00^{+0.61}_{-0.61}$b	$7.50^{+0.12}_{-0.12}$b	200^{+20}_{-20}	$5.4^{+1.9}_{-1.9}$	(4);(25);(25);(4);(6)
080605A	23:47:57.85	Swift/KW	1.64	$19.6^{+0.3}_{-0.3}$b	$4.800^{+0.061}_{-0.061}$b	28^{+14}_{-14}	$0.70^{+0.27}_{-0.27}$	(4);(25);(25);(4);(6)
080604	07:27:01.15	Swift	1.4171	$125.0^{+4.8}_{-4.8}$	$27.0^{+1.2}_{-1.2}$	$1.05^{+0.12}_{-0.12}$	...	(4);(25);(25);(4)
080603B	19:38:13.28	Swift/KW	2.69	$59.50^{+0.48}_{-0.48}$	$6.20^{+0.18}_{-0.18}$b	$6.0^{+3.1}_{-3.1}$	...	(4);(25);(25);(4)
080520A	22:20:24.77	Swift	1.545	$3.00^{+0.24}_{-0.24}$b	$0.510^{+0.048}_{-0.048}$	$0.110^{+0.88}_{-0.024}$ b	$4.1^{+1.6}_{-1.6}$	(25);(25);(25);(25);(6)
080516	00:17:07.03	Swift	3.2	$6.80^{+0.18}_{-0.18}$b	$1.00^{+0.12}_{-0.12}$b	$12.0^{+6}_{-4.8}$	...	(10);(25);(25);(27)
080430	19:53:02.07	Swift	0.767	$16.00^{+0.61}_{-0.61}$b	$3.400^{+0.061}_{-0.061}$b	$0.380^{+0.18}_{-0.048}$ b	$0.81^{+0.37}_{-0.37}$	(25);(25);(25);(25);(6)
080413B	08:51:12.54	Swift	1.1	$7.00^{+0.42}_{-0.42}$b	$1.16^{+0.03}_{-0.03}$b	$1.61^{+0.27}_{-0.27}$	...	(4);(25);(25);(4)
080413A	02:54:19.30	Swift/AGILE/Suzaku	2.433	$46.60^{+0.12}_{-0.12}$b	$5.30^{+0.12}_{-0.12}$b	$8.6^{+2.1}_{-2.1}$	...	(4);(25);(25);(4)
080411A	21:15:32.58	Swift/KW	1.03	$58.30^{+0.48}_{-0.48}$b	$6.700^{+0.061}_{-0.061}$b	$16.2^{+1.6}_{-1.6}$	...	(4);(25);(25);(4)
080330A	03:41:16.87	Swift	1.51	$66.00^{+0.61}_{-0.61}$b	$4.00^{+0.36}_{-0.36}$	$0.410^{+0.57}_{-0.036}$ b	...	(25);(25);(25);(25)
080325A	04:09:17.33	Swift	1.78	$184.0^{+5.4}_{-5.4}$b	$41.0^{+2.4}_{-2.4}$b	$9.55^{+0.84}_{-0.84}$	$6.0^{+0.7}_{-0.7}$	(4);(25);(25);(4);(6)

Table 3 (*continued*)

GRB	Time	Instrument	z	T_{90} (s)	T_{R45} (s)	$E_{\gamma,\mathrm{iso}}$ (10^{52} ergs)	offset (kpc)	ref
080320	04:37:38.46	Swift	7	$21.0^{+1.8}_{-1.8}$ [b]	$4.1^{+0.3}_{-0.3}$ [b]	$34.2^{+46}_{-5.7}$	...	(31);(25);(25);(28)
080319C	12:25:56.96	Swift/AGILE	1.95	33^{+3}_{-3} [b]	$5.00^{+0.18}_{-0.18}$ [b]	$14.9^{+3.0}_{-3.0}$	$7.4^{+0.4}_{-0.4}$	(4);(25);(25);(4);(6)
080319B	06:12:49.25	Swift/KW	0.937	$147.0^{+2.4}_{-2.4}$	$20.300^{+0.061}_{-0.061}$ [b]	118^{+12}_{-12}	$1.72^{+0.95}_{-0.95}$	(4);(25);(25);(4);(6)
080319A	05:45:42.05	Swift	2.0265	$46.0^{+1.2}_{-1.2}$ [b]	$13.30^{+0.54}_{-0.54}$ [b]	$29.2^{+25.5}_{-3.7}$	...	(29);(25);(25);(28)
080310A	08:37:58.64	Swift	2.4274	$362.0^{+3.6}_{-3.6}$ [b]	$24.00^{+0.61}_{-0.61}$ [b]	$8.58^{+0.90}_{-0.90}$	...	(4);(25);(25);(4)
080210A	07:50:05.43	Swift	2.6419	$44.0^{+4.2}_{-4.2}$ [b]	$8.80^{+0.36}_{-0.36}$ [b]	$4.77^{+0.29}_{-0.29}$	...	(4);(25);(25);(4)
080207A	21:30:21.44	Swift	2.0858	$310.0^{+9.1}_{-9.1}$ [b]	$70.0^{+6.1}_{-6.1}$ [b]	$16.4^{+1.8}_{-1.8}$	$6.6^{+3.7}_{-3.7}$	(4);(25);(25);(4);(6)
080129	06:06:45.46	Swift	4.349	$46.0^{+2.4}_{-2.4}$ [b]	$10.00^{+0.61}_{-0.61}$ [b]	$8.0^{+4.2}_{-2.4}$ [b]	...	(25);(25);(25);(25
080123	04:21:57.40	Swift/INTEGRAL	0.495	$26.0^{+2.4}_{-2.4}$ [b]	$3.10^{+0.48}_{-0.48}$ [b]	$0.117^{+0.039}_{-0.039}$	...	(4);(25);(25);(4)
071227A	20:13:47.04	Swift/INTEGRAL/KW	0.383	$2.20^{+0.18}_{-0.18}$ [b]	$0.500^{+0.036}_{-0.036}$ [b]	$0.08^{+0.01}_{-0.01}$	$15.7^{+0.3}_{-0.3}$	(7);(25);(25);(4);(6)
071122	01:23:25.62	Swift	1.14	$79.0^{+4.8}_{-4.8}$ [b]	$16.0^{+1.2}_{-1.2}$ [b]	$0.300^{+0.3}_{-0.061}$ [b]	$0.63^{+0.45}_{-0.45}$	(25);(25);(25);(25);(6)
071117	14:50:06.91	Swift/KW	1.331	$1.700^{+0.061}_{-0.061}$ [b]	$1.28^{+0.03}_{-0.03}$ [b]	$5.86^{+2.70}_{-2.70}$	...	(4);(25);(25);(4)
071112C	18:32:57	Swift	0.8227	15 [a]	...	4.14 [a]	$1.55^{+0.21}_{-0.21}$	(6);(6);(6);(6)
071031A	01:06:36.96	Swift	2.6918	$190.0^{+6.7}_{-6.7}$ [b]	$34.0^{+2.4}_{-2.4}$ [b]	$4.99^{+0.97}_{-0.97}$	...	(4);(25);(25);(4)
071025	04:08:53.68	Swift	5.2	$161.0^{+4.8}_{-4.8}$ [b]	$39.00^{+0.61}_{-0.61}$ [b]	428^{+285}_{-86}	...	(15);(25);(25);(28)
071020	07:02:26.94	Swift	2.145	$4.40^{+0.24}_{-0.24}$ [b]	$1.360^{+0.018}_{-0.018}$ [b]	$10.0^{+4.6}_{-4.6}$	...	(4);(25);(25);(4)
071011	12:40:13.00	Swift	5	$87.0^{+4.8}_{-4.8}$ [b]	$18.00^{+0.61}_{-0.61}$ [b]	234^{+182}_{-104}	...	(31);(25);(25);(28)
071010A	03:41:11.85	Swift	0.98	$22.0^{+1.2}_{-1.2}$ [b]	$1.80^{+0.24}_{-0.24}$ [b]	$0.130^{+0.15}_{-0.012}$ [b]	0.34 [a]	(25);(25);(25);(25);(23)
071010B	20:45:47.98	Swift/KW	0.947	$35.00^{+0.61}_{-0.61}$ [b]	$4.700^{+0.061}_{-0.061}$ [b]	$2.3^{+0.4}_{-0.4}$	$0.88^{+0.20}_{-0.20}$	(4);(25);(25);(4);(6)
071003	07:40:55.01	Swift/INTEGRAL/KW	1.604	$148.00^{+0.61}_{-0.61}$ [b]	$10.3^{+0.3}_{-0.3}$ [b]	$38.3^{+4.5}_{-4.5}$	...	(4);(25);(25);(4)
070810A	02:11:52.41	Swift	2.17	$7.70^{+0.42}_{-0.42}$ [b]	$2.50^{+0.12}_{-0.12}$ [b]	$0.900^{+0.18}_{-0.061}$ [b]	...	(25);(25);(25);(25
070809	19:22:17.37	Swift	0.473	$0.76^{+0.03}_{-0.03}$ [b]	$0.260^{+0.018}_{-0.018}$ [b]	$0.0276^{+0.0037}_{-0.0037}$	$20.0^{+1.6}_{-1.6}$	(4);(25);(25);(4);(6)
070802A	07:07:25.87	Swift	2.45	$15.00^{+0.61}_{-0.61}$ [b]	$3.50^{+0.24}_{-0.24}$ [b]	$0.500^{+0.32}_{-0.061}$ [b]	$1.1^{+0.4}_{-0.4}$	(25);(25);(25);(25);(6)
070729	00:25:53.91	Swift	0.8	$1.000^{+0.061}_{-0.061}$ [b]	$0.300^{+0.024}_{-0.024}$ [b]	$0.113^{+0.044}_{-0.044}$	...	(4);(25);(25);(4)
070724A	10:53:50.21	Swift	0.457	$0.600^{+0.061}_{-0.061}$ [b]	$0.110^{+0.012}_{-0.012}$ [b]	$0.0060^{+0.0014}_{-0.0014}$	$5.5^{+0.2}_{-0.2}$	(7);(25);(25);(4);(6)
070721B	10:33:48.00	Swift	3.6298	$330.0^{+6.1}_{-6.1}$ [b]	$17.00^{+0.61}_{-0.61}$ [b]	$24.2^{+1.4}_{-1.4}$	...	(4);(25);(25);(4)
070714B	04:59:29.62	Swift	0.923	$64.0^{+1.2}_{-1.2}$ [b]	$1.40^{+0.12}_{-0.12}$ [b]	$0.98^{+0.24}_{-0.24}$	$12.4^{+0.9}_{-0.9}$	(4);(25);(25);(4);(6)
070612A	02:38:45.98	Swift	0.617	255^{+3}_{-3} [b]	$62.0^{+1.8}_{-1.8}$ [b]	$2.00^{+1.1}_{-0.24}$ [b]	...	(25);(25);(25);(25
070611	01:57:13.89	Swift	2.0394	$11.30^{+0.42}_{-0.42}$ [b]	$2.60^{+0.18}_{-0.18}$ [b]	$0.92^{+0.13}_{-0.13}$	...	(4);(25);(25);(4)
070529	12:48:28.34	Swift	2.4996	$112.0^{+2.4}_{-2.4}$ [b]	$23.0^{+1.2}_{-1.2}$ [b]	$12.8^{+1.1}_{-1.1}$	...	(4);(25);(25);(4)
070521	06:51:10.86	Swift/KW	1.35	$560.0^{+6.1}_{-6.1}$ [b]	$10.60^{+0.36}_{-0.36}$ [b]	$10.8^{+1.8}_{-1.8}$	...	(4);(25);(25);(4)
070518	14:26:21.20	Swift/KW	1.16	$5.30^{+0.18}_{-0.18}$ [b]	$1.200^{+0.061}_{-0.061}$ [b]	$0.0900^{+0.091}_{-0.0061}$ [b]	...	(25);(25);(25);(25)
070508	04:18:17.83	Swift	0.82	$21.20^{+0.24}_{-0.24}$ [b]	$5.200^{+0.018}_{-0.018}$ [b]	$7.74^{+0.29}_{-0.29}$	$3.3^{+0.3}_{-0.3}$	(4);(32);(32);(4);(6)
070506A	05:35:58.06	Swift	2.31	$3.60^{+0.18}_{-0.18}$ [b]	$1.000^{+0.061}_{-0.061}$ [b]	$0.513^{+0.054}_{-0.054}$	...	(4);(32);(32);(4)
070429B	03:09:04.44	Swift	0.904	$0.3200^{+0.0061}_{-0.0061}$ [b]	$0.080^{+0.012}_{-0.012}$ [b]	$0.0475^{+0.0071}_{-0.0071}$	4.7 [a]	(7);(32);(32);(4);(19)
070419B	10:44:05.97	Swift	1.96	134^{+3}_{-3} [b]	$41.00^{+0.61}_{-0.61}$ [b]	$15.7^{+11}_{-2.9}$	...	(15);(32);(32);(27)
070419A	09:59:26.09	Swift	0.97	$160.0^{+8.5}_{-8.5}$ [b]	$37.0^{+2.4}_{-2.4}$ [b]	$0.24^{+0.10}_{-0.10}$	...	(4);(32);(32);(4)
070411A	20:12:33.00	Swift	2.954	109^{+3}_{-3} [b]	$32.00^{+0.61}_{-0.61}$ [b]	$8.31^{+0.45}_{-0.45}$	...	(4);(32);(32);(4)
070328A	03:53:53.15	Swift/KW	2.0627	$50.00^{+0.61}_{-0.61}$ [b]	$12.70^{+0.12}_{-0.12}$ [b]	64 [a]	...	(33);(32);(32);(33)
070318A	07:28:56.08	Swift	0.84	$51.0^{+1.8}_{-1.8}$ [b]	$10.3^{+0.3}_{-0.3}$ [b]	$3.64^{+0.17}_{-0.17}$	$0.84^{+0.47}_{-0.47}$	(4);(32);(32);(4);(6)
070306A	16:41:28.17	Swift	1.4959	260^{+12}_{-12} [b]	$16.00^{+0.61}_{-0.61}$ [b]	$8.26^{+0.41}_{-0.41}$	$0.78^{+0.39}_{-0.39}$	(4);(32);(32);(4);(6)
070208	09:10:34.28	Swift	1.165	$52.00^{+0.61}_{-0.61}$ [b]	$4.60^{+0.48}_{-0.48}$ [b]	$0.280^{+0.13}_{-0.048}$ [b]	$0.83^{+0.34}_{-0.34}$	(32);(32);(32);(32);(6)
070129A	23:35:10.26	Swift	2.34	$92.0^{+1.8}_{-1.8}$ [b]	$28.00^{+0.61}_{-0.61}$ [b]	$2.89^{+1.2}_{-0.55}$	...	(15);(32);(32);(27)
070110A	07:22:41.57	Swift	2.3521	$48.0^{+1.2}_{-1.2}$ [b]	$16.20^{+0.54}_{-0.54}$ [b]	$5.0^{+0.3}_{-0.3}$	...	(4);(32);(32);(4)
070103A	20:46:39.41	Swift	2.62	$10.90^{+0.12}_{-0.12}$ [b]	$1.50^{+0.18}_{-0.18}$ [b]	$0.58^{+0.59}_{-0.14}$	...	(15);(32);(32);(27)
061222B	04:11:02.35	Swift	3.355	$42.0^{+1.8}_{-1.8}$ [b]	$12.40^{+0.54}_{-0.54}$ [b]	$8.0^{+4.2}_{-1.2}$ [b]	...	(32);(32);(32);(32
061222A	03:28:52.11	Swift/KW	2.088	$82.0^{+3.6}_{-3.6}$ [b]	$9.00^{+0.12}_{-0.12}$ [b]	$30.0^{+6.4}_{-6.4}$	...	(4);(32);(32);(4)
061217	03:40:08.21	Swift	0.827	$0.350^{+0.036}_{-0.036}$ [b]	$0.1000^{+0.0061}_{-0.0061}$ [b]	$0.423^{+0.072}_{-0.072}$	55^{+28}_{-28}	(7);(32);(32);(4);(34)
061210A	12:20:39.33	Swift	0.409	$0.100^{+0.012}_{-0.012}$ [b]	$0.0400^{+0.0061}_{-0.0061}$ [b]	$0.0024^{+0.0006}_{-0.0006}$	$10.7^{+9.7}_{-9.7}$	(4);(32);(32);(4);(34)
061201	15:58:36.82	Swift/KW	0.111	$0.86^{+0.03}_{-0.03}$ [b]	$0.220^{+0.012}_{-0.012}$ [b]	$0.0151^{+0.0073}_{-0.0073}$	$32.9^{+0.1}_{-0.1}$	(7);(32);(32);(4);(6)
061126	08:47:56.42	Swift/RHESSI	1.1588	$26.80^{+0.48}_{-0.48}$ [b]	$5.50^{+0.12}_{-0.12}$ [b]	$31.4^{+3.6}_{-3.6}$	...	(4);(32);(32);(4)
061121	15:22:29.00	Swift/KW	1.314	80^{+13}_{-13} [b]	$5.800^{+0.061}_{-0.061}$ [b]	$23.5^{+2.7}_{-2.7}$	...	(4);(32);(32);(4)
061110B	21:58:45.54	Swift	3.4344	$32.40^{+0.61}_{-0.61}$ [b]	$8.60^{+0.36}_{-0.36}$ [b]	$17.9^{+1.6}_{-1.6}$	$0.46^{+0.23}_{-0.23}$	(4);(32);(32);(4);(6)
061110A	11:47:21.31	Swift	0.758	$47.0^{+1.2}_{-1.2}$ [b]	$15.00^{+0.61}_{-0.61}$ [b]	$0.280^{+0.17}_{-0.036}$ [b]	$1.01^{+0.30}_{-0.30}$	(10);(32);(32);(35);(6)
061028	01:26:22.46	Swift	0.76	120^{+11}_{-11} [b]	$19.0^{+1.2}_{-1.2}$ [b]	0.229 [a]	...	(36);(32);(32);(36)
061021A	15:39:07.00	Swift	0.3462	$12.1^{+0.3}_{-0.3}$ [b]	$2.500^{+0.061}_{-0.061}$ [b]	$0.50^{+0.11}_{-0.11}$	...	(4);(32);(32);(4)
061007A	10:08:08.81	Swift/KW	1.262	$74.90^{+0.54}_{-0.54}$ [b]	$16.80^{+0.12}_{-0.12}$ [b]	90^{+9}_{-9}	2.11 [a]	(4);(32);(32);(4);(23)
061006A	16:45:50.51	Swift/INTEGRAL/KW	0.438	$51.0^{+1.2}_{-1.2}$ [b]	$1.80^{+0.12}_{-0.12}$ [b]	$0.179^{+0.056}_{-0.056}$	$1.32^{+0.25}_{-0.25}$	(4);(32);(32);(4);(6)
061004	19:50:30.51	Swift	3.3	$6.5^{+0.3}_{-0.3}$ [b]	$1.620^{+0.054}_{-0.054}$ [b]	$2.00^{+0.67}_{-0.18}$ [b]	...	(32);(32);(32);(32)
060927A	14:07:35.29	Swift	5.46	$23.00^{+0.24}_{-0.24}$ [b]	$3.20^{+0.12}_{-0.12}$ [b]	$12.0^{+2.8}_{-2.8}$	...	(4);(32);(32);(4)
060926A	16:48:41.85	Swift	3.2086	$7.10^{+0.42}_{-0.42}$ [b]	$1.500^{+0.061}_{-0.061}$ [b]	$2.29^{+0.37}_{-0.37}$	...	(4);(32);(32);(4)
060923A	05:12:15.37	Swift	2.8	$57.0^{+1.8}_{-1.8}$ [b]	$5.20^{+0.42}_{-0.42}$ [b]	$20.0^{+9.2}_{-4.6}$	$2.40^{+0.54}_{-0.54}$	(15);(32);(32);(28);(6)

(*continued on next page*)

Table 3 (continued)

GRB	Time	Instrument	z	T_{90} (s)	T_{R45} (s)	$E_{\gamma,iso}$ (10^{52} ergs)	offset (kpc)	ref
060912A	13:55:54.14	Swift	0.937	$5.90^{+0.36}_{-0.36}$[b]	$1.120^{+0.042}_{-0.042}$[b]	$0.80^{+0.3}_{-0.12}$ [b]	$5.2^{+1.2}_{-1.2}$	(32);(32);(32);(32);(6)
060908A	08:57:22.34	Swift	1.884	$18.50^{+0.18}_{-0.18}$	$5.30^{+0.12}_{-0.12}$	$7.2^{+1.9}_{-1.9}$	...	(4);(32);(32);(4)
060906A	08:32:46.57	Swift	3.6856	$70.0^{+9.1}_{-9.1}$[b]	$12.50^{+0.54}_{-0.54}$[b]	$7.81^{+0.51}_{-0.51}$	...	(4);(32);(32);(4)
060904B	02:31:03.85	Swift	0.7029	$171.0^{+1.8}_{-1.8}$	$5.90^{+0.36}_{-0.36}$	$2.4^{+0.2}_{-0.2}$	...	(11);(32);(32);(11)
060814A	23:02:19.03	Swift/KW	1.923	$159.0^{+4.2}_{-4.2}$[b]	$25.80^{+0.42}_{-0.42}$[b]	$56.7^{+5.7}_{-5.7}$	...	(4);(32);(32);(4)
060805A	04:47:49.16	Swift	2.3633	$11.0^{+1.2}_{-1.2}$[b]	$1.00^{+0.12}_{-0.12}$[b]	$1.8^{+2.7}_{-0.5}$	...	(37);(32);(32);(28)
060801A	12:16:15.15	Swift	1.13	$0.700^{+0.061}_{-0.061}$[b]	$0.180^{+0.018}_{-0.018}$[b]	$3.27^{+0.49}_{-0.49}$	17.6[a]	(4);(32);(32);(4);(19)
060729A	19:12:29.24	Swift	0.54	$120.0^{+1.2}_{-1.2}$[b]	$18.00^{+0.61}_{-0.61}$	$1.6^{+0.6}_{-0.6}$	$2.18^{+0.27}_{-0.27}$	(15);(32);(32);(11);(6)
060719A	06:50:36.94	Swift	1.532	$57.00^{+0.61}_{-0.61}$[b]	$5.80^{+0.18}_{-0.18}$	$1.60^{+1.9}_{-0.25}$	$1.79^{+0.70}_{-0.70}$	(10);(32);(32);(27);(6)
060714A	15:12:00.28	Swift	2.7108	$119.0^{+1.8}_{-1.8}$[b]	$22.00^{+0.61}_{-0.61}$	$7.70^{+0.44}_{-0.44}$	...	(4);(32);(32);(4)
060708	12:15:59.01	Swift	1.92	$7.50^{+0.48}_{-0.48}$[b]	$1.900^{+0.061}_{-0.061}$[b]	$1.06^{+0.08}_{-0.08}$	...	(4);(32);(32);(4)
060707A	21:30:19.49	Swift	3.424	$75.0^{+1.8}_{-1.8}$	$14.00^{+0.61}_{-0.61}$	$4.3^{+1.1}_{-1.1}$	...	(4);(32);(32);(4)
060614A	12:43:48.50	Swift/KW	0.125	$109.00^{+0.61}_{-0.61}$[b]	$27.20^{+0.36}_{-0.36}$[b]	$0.217^{+0.087}_{-0.087}$	$0.80^{+0.03}_{-0.03}$	(4);(32);(32);(4);(6)
060607A	05:12:13.35	Swift	3.075	$103.0^{+2.4}_{-2.4}$[b]	$15.10^{+0.48}_{-0.48}$[b]	$11.9^{+2.8}_{-2.8}$	...	(4);(32);(32);(4)
060605A	18:15:44.61	Swift	3.773	$19.00^{+0.61}_{-0.61}$[b]	$5.4^{+0.3}_{-0.3}$[b]	$4.23^{+0.61}_{-0.61}$	$1.35^{+0.86}_{-0.86}$	(4);(32);(32);(4);(6)
060604A	18:19:00.01	Swift	2.14	$40.00^{+0.61}_{-0.61}$[b]	$2.00^{+0.24}_{-0.24}$	$0.50^{+0.12}_{-0.1}$	...	(15);(32);(32);(35)
060602A	21:32:12	Swift	0.787	$77.0^{+4.2}_{-4.2}$[b]	$21.00^{+0.61}_{-0.61}$	1.54[a]	1.21[a]	(10);(32);(32);(6);(23)
060526A	16:28:29.95	Swift	3.22	$296.0^{+4.2}_{-4.2}$[b]	$14.00^{+0.61}_{-0.61}$	$2.75^{+0.37}_{-0.37}$	...	(4);(32);(32);(4)
060522	02:11:18.79	Swift	5.11	$74.0^{+2.4}_{-2.4}$[b]	$20.0^{+1.2}_{-1.2}$	$6.47^{+0.63}_{-0.63}$	1.93[a]	(4);(32);(32);(4);(6)
060512A	23:13:20.73	Swift	2.1	$8.40^{+0.36}_{-0.18}$	$1.90^{+0.18}_{-0.18}$	$0.0200^{+0.018}_{-0.0024}$ [b]	...	(15);(32);(32);(32)
060510B	08:22:14.81	Swift	4.9	$230.0^{+2.4}_{-2.4}$[b]	$79.0^{+1.8}_{-1.8}$	$19.1^{+0.8}_{-0.8}$	...	(4);(32);(32);(4)
060505A	06:36:01	Swift	0.089	$4.00^{+0.61}_{-0.61}$[b]	...	$0.0235^{+0.0042}_{-0.0042}$	$7.2^{+0.1}_{-0.1}$	(38);(38);(4);(6)
060502B	17:24:41.07	Swift	0.287	$0.160^{+0.018}_{-0.018}$[b]	$0.0400^{+0.0061}_{-0.0061}$[b]	$0.0433^{+0.0053}_{-0.0053}$	70^{+16}_{-16}	(7);(32);(32);(4);(34)
060502A	03:03:32.14	Swift	1.51	30^{+3}_{-3}[b]	$8.60^{+0.24}_{-0.24}$	$3.20^{+1.7}_{-0.54}$ [b]	$0.44^{+0.20}_{-0.20}$	(32);(32);(32);(32);(6)
060428B	08:54:38.00	Swift	0.348	$20.00^{+0.61}_{-0.61}$[b]	$7.40^{+0.42}_{-0.42}$[b]	$0.0200^{+0.012}_{-0.0024}$ [b]	...	(32);(32);(32);(32)
060418A	03:06:08.20	Swift/KW	1.489	100^{+10}_{-10}[b]	$14.5^{+0.3}_{-0.3}$[b]	$13.5^{+2.7}_{-2.7}$	$3.5^{+0.0}_{-0.0}$	(4);(32);(32);(4);(6)
060306A	00:49:10.00	Swift	3.5	$61.00^{+0.61}_{-0.61}$[b]	$3.60^{+0.18}_{-0.18}$	$7.6^{+1.0}_{-1.0}$	...	(4);(32);(32);(4)
060223A	06:04:23.00	Swift	4.41	$8.40^{+0.24}_{-0.24}$[b]	$2.60^{+0.12}_{-0.12}$	$3.10^{+0.73}_{-0.6}$[b]	...	(32);(32);(32);(32)
060218A	03:34:30.00	Swift	0.033	$128.0^{+2.4}_{-2.4}$[b]	$34.0^{+1.8}_{-1.8}$[b]	$0.0054^{+0.0005}_{-0.0005}$	$0.116^{+0.030}_{-0.030}$	(4);(32);(32);(4);(6)
060210A	04:58:50.00	Swift	3.91	370^{+21}_{-21}[b]	$36.0^{+1.2}_{-1.2}$[b]	$32.2^{+3.2}_{-3.2}$	...	(4);(32);(32);(4)
060206A	04:46:53.27	Swift	4.056	$6.10^{+0.18}_{-0.18}$[b]	$1.920^{+0.048}_{-0.048}$[b]	$4.1^{+1.9}_{-1.9}$	$2.09^{+0.92}_{-0.92}$	(4);(32);(32);(4);(6)
060202A	08:40:55.00	Swift	0.785	$206.0^{+2.4}_{-2.4}$[b]	$59.0^{+2.4}_{-2.4}$[b]	$1.20^{+0.09}_{-0.09}$	$11.6^{+8.3}_{-8.3}$	(4);(32);(32);(4);(6)
060124A	15:54:51.82	Swift/KW	2.296	$8.20^{+0.18}_{-0.18}$[b]	$2.40^{+0.18}_{-0.18}$	$43.8^{+6.4}_{-6.4}$	$1.11^{+0.77}_{-0.77}$	(4);(32);(32);(4);(6)
060121A	22:24:54.50	HETE-2/KW	$1.92^{+0.35}_{-0.35}$	$2.61^{+0.10}_{-0.10}$	...	...	$0.73^{+0.37}_{-0.37}$	(39);(6);(6)
060116	08:37:27.23	Swift	6.6	$36.00^{+0.61}_{-0.61}$[b]	$9.60^{+0.48}_{-0.48}$[b]	$21.0^{+9.7}_{-4.2}$[b]	...	(32);(32);(32);(32)
060115A	13:08:00.64	Swift	3.533	$110.00^{+0.61}_{-0.61}$[b]	$16.00^{+0.61}_{-0.61}$	$5.9^{+3.8}_{-3.8}$	$2.11^{+0.49}_{-0.49}$	(4);(32);(32);(4);(6)
060111B	20:15:43.24	Swift	1.5	$61.0^{+1.2}_{-1.2}$	$11.00^{+0.61}_{-0.61}$	$2.9^{+5.2}_{-1.3}$	...	(40);(32);(32);(41)
060110	08:01:17.77	Swift	5	$24.0^{+1.2}_{-1.2}$	$5.60^{+0.12}_{-0.12}$	83^{+68}_{-16}	...	(31);(5);(32);(28)
060108	14:39:11.76	Swift	2.7	$15.0^{+1.2}_{-1.2}$[b]	$3.40^{+0.18}_{-0.18}$	$0.59^{+0.84}_{-0.08}$	...	(15);(32);(32);(35)
051227	18:07:16.00	Swift	0.714	$35.50^{+0.54}_{-0.54}$[b]	$2.50^{+0.18}_{-0.18}$	$0.120^{+0.097}_{-0.03}$[b]	...	(32);(32);(32);(32)
051221A	01:51:16.00	Swift/INTEGRAL/KW	0.547	$1.240^{+0.024}_{-0.024}$[b]	$0.1600^{+0.0061}_{-0.0061}$[b]	$0.263^{+0.033}_{-0.033}$	$1.95^{+0.19}_{-0.19}$	(7);(32);(32);(4);(6)
051210A	05:46:21.16	Swift	1.4	$1.60^{+0.12}_{-0.12}$[b]	$0.32^{+0.03}_{-0.03}$	...	36^{+15}_{-15}	(6);(32);(32);(6)
051117B	13:22:54.42	Swift	0.48	$10.5^{+0.3}_{-0.3}$[b]	$2.10^{+0.18}_{-0.18}$[b]	$0.018^{+0.02}_{-0.005}$	...	(15);(32);(32);(27)
051111	05:59:41.47	Swift	1.55	$51.0^{+2.4}_{-2.4}$[b]	$9.90^{+0.24}_{-0.24}$	$15.4^{+1.9}_{-1.9}$	...	(4);(32);(32);(4)
051109B	08:39:39.00	Swift	0.08	$8.30^{+0.42}_{-0.42}$[b]	$1.90^{+0.18}_{-0.18}$	$0.000360^{+0.00012}_{-0.000054}$ [b]	...	(32);(32);(32);(32)
051109A	01:12:20.00	Swift/KW	2.346	$4.9^{+0.3}_{-0.3}$	$1.300^{+0.061}_{-0.061}$[b]	$6.85^{+0.73}_{-0.73}$	...	(4);(32);(32);(4)
051022A	13:07:58.49	HETE-2/KW	0.8	178^{+8}_{-8}	$10.30^{+0.23}_{-0.23}$	$56.0^{+5.6}_{-5.6}$	$1.31^{+0.95}_{-0.95}$	(4);(39);(42);(4);(6)
051016B	18:28:09.00	Swift	0.9364	$1.400^{+0.061}_{-0.061}$[b]	$0.48^{+0.03}_{-0.03}$	$0.0370^{+0.034}_{-0.0036}$ [b]	$2.1^{+1.6}_{-1.6}$	(32);(32);(32);(32);(6)
051008A	16:33:21.00	Swift	2.9	$45.00^{+0.61}_{-0.61}$[b]	$8.60^{+0.24}_{-0.24}$	$9.6^{+1.5}_{-1}$	...	(43);(32);(32);(27)
051001A	11:11:36.00	Swift	2.43	$56.0^{+1.2}_{-1.2}$[b]	$20.00^{+0.61}_{-0.61}$	$2.09^{+0.56}_{-0.29}$	...	(15);(32);(32);(27)
050922C	19:55:50.00	Swift/HETE-2/KW	2.199	$4.60^{+0.12}_{-0.12}$[b]	$1.200^{+0.024}_{-0.024}$[b]	$5.6^{+1.8}_{-1.8}$	...	(4);(32);(32);(4)
050911	15:59:34.00	Swift	0.165	$16.30^{+0.12}_{-0.12}$[b]	$1.10^{+0.12}_{-0.12}$[b]	$0.0089^{+0.0016}_{-0.0016}$	...	(4);(32);(32);(4)
050908	05:42:31.00	Swift	3.347	$10.80^{+0.54}_{-0.54}$[b]	$3.40^{+0.18}_{-0.18}$	$1.54^{+0.16}_{-0.16}$	...	(4);(32);(32);(4)
050904A	01:51:44.00	Swift	6.295	$197.0^{+1.8}_{-1.8}$[b]	$71.0^{+1.2}_{-1.2}$[b]	133^{+14}_{-14}	$0.75^{+0.23}_{-0.23}$	(4);(32);(32);(4);(6)
050826A	06:18:10.00	Swift	0.297	$34.0^{+1.8}_{-1.8}$[b]	$5.20^{+0.36}_{-0.36}$[b]	$0.030^{+0.024}_{-0.012}$[b]	1.777[a]	(32);(32);(32);(32);(6)
050824A	23:12:16.00	Swift	0.83	38^{+3}_{-3}[b]	$7.00^{+0.61}_{-0.61}$[b]	$0.150^{+0.52}_{-0.024}$ [b]	$3.6^{+0.4}_{-0.4}$	(32);(32);(32);(32);(6)
050822	03:49:29.00	Swift	1.43	105^{+3}_{-3}[b]	$16.00^{+0.61}_{-0.61}$	$2.55^{+3.2}_{-0.26}$	...	(15);(32);(32);(27)
050820A	06:34:53.00	Swift/KW	2.615	$239.70^{+0.36}_{-0.36}$[b]	$11.00^{+0.48}_{-0.48}$[b]	103^{+10}_{-10}	$3.6^{+0.1}_{-0.1}$	(4);(32);(32);(4);(6)
050819A	16:23:55.00	Swift	2.5	47^{+3}_{-3}[b]	$8.00^{+0.61}_{-0.61}$[b]	$1.02^{+1.5}_{-0.34}$	...	(15);(32);(32);(27)
050814	11:38:57.00	Swift	5.3	$28.0^{+1.8}_{-1.8}$[b]	$10.00^{+0.61}_{-0.61}$	$9.9^{+1.1}_{-1.1}$	...	(4);(32);(32);(4)
050813	06:45:09.80	Swift	0.72	$0.500^{+0.012}_{-0.012}$[b]	$0.090^{+0.012}_{-0.012}$[b]	$0.0150^{+0.015}_{-0.0048}$ [b]	35.5[a]	(32);(32);(32);(32);(19)
050803	19:14:00.00	Swift	$4.3^{+0.6}_{-2.4}$	$88.0^{+1.2}_{-1.2}$[b]	$17.00^{+0.61}_{-0.61}$	$0.24^{+0.24}_{-0.08}$	...	(29);(32);(32);(35)
050802A	10:08:02.00	Swift	1.71	$14.30^{+0.61}_{-0.61}$[b]	$4.10^{+0.18}_{-0.18}$[b]	$5.66^{+0.47}_{-0.47}$	...	(4);(32);(32);(4)

Table 3 (*continued*)

GRB	Time	Instrument	z	T_{90} (s)	T_{R45} (s)	$E_{\gamma,\mathrm{iso}}$ (10^{52} ergs)	offset (kpc)	ref
050801	18:28:02.07	Swift	1.38	$5.9^{+0.3}_{-0.3}$[b]	$1.000^{+0.061}_{-0.061}$[b]	$0.41^{+0.64}_{-0.06}$	...	(15);(32);(32);(28)
050730A	19:58:23.00	Swift	3.969	$60.0^{+1.8}_{-1.8}$[b]	$21.00^{+0.61}_{-0.61}$[b]	$11.8^{+0.8}_{-0.8}$	...	(4);(32);(32);(4)
050724A	12:34:09.00	Swift/INTEGRAL	0.257	$92.0^{+1.2}_{-1.2}$[b]	$2.50^{+0.18}_{-0.18}$[b]	$0.0619^{+0.0074}_{-0.0074}$	$2.68^{+0.08}_{-0.08}$	(4);(32);(32);(4);(6)
050713A	04:29:02.39	Swift	3.6	$120.0^{+7.3}_{-7.3}$[b]	$7.70^{+0.18}_{-0.18}$[b]	156^{+132}_{-48}	...	(31);(32);(32);(28)
050709A	22:36:36.70	HETE-2	0.161	0.07[a]	...	$0.0080^{+0.0008}_{-0.0008}$	$3.8^{+0.0}_{-0.0}$	(4);(14);(4);(6)
050607	09:11:23.00	Swift	4	$17.30^{+0.48}_{-0.48}$	$4.40^{+0.18}_{-0.18}$	$12.3^{+11}_{-1.5}$	...	(31);(32);(32);(28)
050603	06:29:05.00	Swift/KW	2.821	$9.80^{+0.36}_{-0.36}$[b]	$1.600^{+0.061}_{-0.061}$[b]	$64.1^{+6.4}_{-6.4}$	...	(4);(32);(32);(4)
050525A	00:02:53.00	Swift/INTEGRAL/KW	0.606	$9.100^{+0.042}_{-0.042}$[b]	$2.60^{+0.03}_{-0.03}$[b]	$2.30^{+0.49}_{-0.49}$	$0.190^{+0.048}_{-0.048}$	(4);(32);(32);(4);(6)
050509B	04:00:19.00	Swift	0.225	$0.0800^{+0.0042}_{-0.0042}$[b]	$0.0200^{+0.0042}_{-0.0042}$	$0.00085^{+0.00022}_{-0.00022}$	$64.8^{+12.4}_{-12.4}$	(4);(32);(32);(4);(6)
050505A	23:22:21.00	Swift	4.27	$60.00^{+0.61}_{-0.61}$[b]	$9.60^{+0.48}_{-0.48}$[b]	$16.0^{+1.1}_{-1.1}$	...	(4);(32);(32);(4)
050502B	09:25:40.00	Swift	5.2	$17.4^{+0.3}_{-0.3}$[b]	$2.10^{+0.12}_{-0.12}$[b]	$2.66^{+0.22}_{-0.22}$	...	(4);(32);(32);(4)
050502A	02:14:17.67	INTEGRAL	3.793	$10.90^{+0.16}_{-0.16}$	$4.60^{+0.28}_{-0.28}$	4^{+3}_{-1}	...	(44);(45);(42);(46)
050416A	11:04:45.00	Swift	0.6535	$2.90^{+0.18}_{-0.18}$[b]	$0.630^{+0.036}_{-0.036}$[b]	$0.100^{+0.03}_{-0.012}$	$0.261^{+0.092}_{-0.092}$	(32);(32);(32);(32);(6)
050406	15:58:48.00	Swift	2.44	$5.00^{+0.61}_{-0.61}$[b]	$0.90^{+0.12}_{-0.12}$[b]	$0.23^{+0.2}_{-0.08}$ [b]	...	(10);(32);(32);(27)
050401A	14:20:15.00	Swift/KW	2.898	$34.4^{+0.3}_{-0.24}$[b]	$5.20^{+0.24}_{-0.24}$[b]	$37.6^{+7.3}_{-7.3}$	$0.66^{+0.41}_{-0.41}$	(4);(32);(32);(4);(6)
050319A	09:31:18.00	Swift	3.243	$154.0^{+1.2}_{-1.2}$[b]	$12.00^{+0.61}_{-0.61}$[b]	$4.63^{+0.56}_{-0.56}$	...	(4);(32);(32);(4)
050318A	15:44:37.00	Swift	1.444	$31.000^{+0.061}_{-0.061}$[b]	$3.50^{+0.12}_{-0.12}$[b]	$2.30^{+0.23}_{-0.23}$	...	(4);(32);(32);(4)
050315	20:59:42.00	Swift	1.95	$95.0^{+1.8}_{-1.8}$[b]	$19.30^{+0.48}_{-0.48}$[b]	$6.15^{+0.30}_{-0.30}$	$0.98^{+0.48}_{-0.48}$	(4);(32);(32);(4);(6)
050223A	03:09:06.00	Swift/INTEGRAL	0.5915	$17.40^{+0.54}_{-0.54}$[b]	$5.1^{+0.3}_{-0.3}$[b]	$0.0700^{+0.03}_{-0.0061}$ [b]	...	(32);(32);(32);(32)
050126	12:00:53.00	Swift	1.29	$29.0^{+1.2}_{-1.2}$[b]	$8.10^{+0.48}_{-0.48}$[b]	$2.47^{+0.25}_{-0.25}$	...	(4);(32);(32);(4)
041006A	12:18:08	HETE-2	0.716	18[a]	$4.26^{+0.12}_{-0.12}$	$3.11^{+0.89}_{-0.89}$	$2.57^{+0.06}_{-0.06}$	(4);(11);(42);(4);(6)
040924A	11:52:11	HETE-2/KW	0.859	2.39[a]	$0.49^{+0.02}_{-0.02}$	$0.98^{+0.10}_{-0.10}$	$2.23^{+0.12}_{-0.12}$	(4);(11);(42);(4);(6)
030528A	13:03:03	HETE-2	0.78	$62.8^{+4.5}_{-4.5}$	$9.99^{+0.93}_{-0.93}$	$2.22^{+0.27}_{-0.27}$	...	(4);(39);(42);(4)
030429A	10:42:23	HETE-2	2.65	$13.0^{+2.7}_{-2.7}$	$2.13^{+0.35}_{-0.35}$	$2.29^{+0.27}_{-0.27}$	8.199[a]	(4);(39);(42);(4);(6)
030329A	11:37:15	HETE-2	0.169	22.76[a]	$4.43^{+0.23}_{-0.23}$	$1.62^{+0.16}_{-0.16}$	...	(4);(11);(42);(4)
030328A	11:20:58	HETE-2	1.52	138^{+3}_{-3}	$20.8^{+0.7}_{-0.7}$	$38.9^{+3.9}_{-3.9}$	...	(4);(39);(42);(4)
030323A	21:56:57.60	HETE-2	3.37	$32.6^{+2.7}_{-2.7}$	$6.9^{+0.7}_{-0.7}$	$2.94^{+0.92}_{-0.92}$	1.072[a]	(4);(47);(42);(4);(6)
030226A	03:46:31.99	HETE-2	1.98	76^{+4}_{-4}	$8.86^{+0.87}_{-0.87}$	$12.7^{+1.4}_{-1.4}$	...	(4);(39);(42);(4)
030115A	03:22:34.28	HETE-2	2.5	$20.3^{+3.5}_{-3.5}$	$4.26^{+0.30}_{-0.30}$	$4.19^{+1.4}_{-0.88}$	...	(44);(39);(42);(44)
021211A	11:18:34.03	HETE-2	1.01	2.8[a]	$0.66^{+0.12}_{-0.12}$	$1.16^{+0.13}_{-0.13}$	...	(4);(11);(42);(4)
021004A	12:06:13.57	HETE-2	2.3	48.9[a]	$6.89^{+0.41}_{-0.41}$	$3.47^{+0.46}_{-0.46}$	2.357[a]	(4);(13);(42);(4);(6)
020813A	02:44:19.17	HETE-2	1.25	87.9[a]	$17.36^{+0.23}_{-0.23}$	68^{+17}_{-17}	...	(4);(13);(42);(4)
020405A	00.41.34	Ulysess/BeppoSAX/Konus	0.69	$40.0^{+2.2}_{-2.2}$	$10.18^{+0.38}_{-0.38}$	$10.6^{+1.1}_{-1.1}$	...	(4);(48);(42);(4)
020124	10:41:15.14	HETE-2	3.2	51.2[a]	$12.14^{+0.58}_{-0.58}$	$28.5^{+2.8}_{-2.8}$	...	(4);(13);(42);(4)
011121A	18:47:08	BeppoSAX	0.36	$47.0^{+3.2}_{-3.2}$	8.3[a]	$8.0^{+2.2}_{-2.2}$	4.563[a]	(4);(48);(49);(4);(6)
010921A	05:15:50	HETE/Ulysess/BeppoSAX	0.45	$22.0^{+3.6}_{-3.6}$	$5.04^{+0.53}_{-0.51}$	$0.97^{+0.10}_{-0.10}$	$1.89^{+0.19}_{-0.19}$	(4);(48);(50);(4);(6)
010222A	07:23:03	BeppoSAX/Konus	1.48	$74.0^{+4.1}_{-4.1}$	$3.42^{+0.62}_{-0.53}$	$84.9^{+9.0}_{-9.0}$	$0.38^{+0.05}_{-0.05}$	(4);(48);(50);(4);(6)
000911A	...	Ulysses/KW/NEAR/IPN	1.06	500[a]	$6.46^{+0.32}_{-0.32}$	70^{+14}_{-14}	...	(4);(11);(42);(4)
000301D	09:51:37	RXTE/Ulysses	2.03	10[a]	...	...	$0.622^{+0.063}_{-0.063}$	(51);(36);(52)
000210A	08:44:05	BeppoSAX/Chandra/Konus	0.846	$9.0^{+1.4}_{-1.4}$	$1.06^{+0.16}_{-0.14}$	$15.4^{+1.7}_{-1.7}$	7.773[a]	(4);(48);(50);(4);(6)
000131	14:57:57.5	Ulysses/KW/CGRO	4.5	110[a]	$4.54^{+0.09}_{-0.09}$	184^{+32}_{-32}	...	(4);(36);(42);(4)
991208A	04:36:52	Ulysses/KW	0.706	60[a]	5.1[a]	$23.0^{+2.3}_{-2.3}$	$1.43^{+0.71}_{-0.71}$	(4);(11);(49);(4);(6)
990712B	16:43:02	BeppoSAX	0.434	$19.0^{+4.5}_{-4.5}$	$3.54^{+0.26}_{-0.25}$	$0.69^{+0.13}_{-0.13}$	...	(4);(48);(50);(4)
990705A	16:01:25	BeppoSAX/Konus	0.842	$32.0^{+1.4}_{-1.4}$	$7.94^{+1.1}_{-0.95}$	$18.7^{+2.7}_{-2.7}$	$6.8^{+0.4}_{-0.4}$	(4);(48);(50);(4);(6)
990510A	08:49:06.3	BeppoSAX/CGRO	1.619	67.6[a]	$1.53^{+0.24}_{-0.22}$	$18.1^{+2.7}_{-2.7}$	$0.57^{+0.08}_{-0.08}$	(4);(13);(50);(4);(6)
990506A	11:23:30.9	RXTE/CGRO/BeppoSAX	1.3	$129.0^{+1.4}_{-1.4}$	$4.84^{+0.9}_{-0.76}$	$98.1^{+9.9}_{-9.9}$	...	(4);(48);(50);(4)
990123A	09:46:56.1	BeppoSAX/CGRO	1.6	$63.36^{+0.26}_{-0.26}$	$6.5^{+1.4}_{-1.1}$	241^{+39}_{-39}	$5.8^{+0.0}_{-0.0}$	(4);(53);(50);(4);(6)
980703A	04:22:45.2	RXTE/CGRO/BeppoSAX	0.966	$411.6^{+9.3}_{-9.3}$	$11.5^{+2.7}_{-2.5}$	$7.42^{+0.74}_{-0.74}$	$0.91^{+0.51}_{-0.51}$	(4);(53);(50);(4);(6)
980613A	04:51:06	BeppoSAX	1.096	42^{+22}_{-22}	...	$0.5^{+0.1}_{-0.1}$	$0.74^{+0.63}_{-0.63}$	(4);(48);(4);(6)
980425A	21:49:08.7	CGRO/BeppoSAX	0.0085	$18.0^{+4.1}_{-4.1}$	$4.46^{+0.29}_{-0.29}$	$0.000064^{+0.000016}_{-0.000016}$	$2.19^{+0.01}_{-0.01}$	(4);(48);(50);(4);(6)
971214B	23:20:41.2	BeppoSAX/CGRO	3.42	$30.0^{+6.3}_{-6.3}$	$1.45^{+0.39}_{-0.31}$	$22.1^{+2.7}_{-2.7}$	$1.11^{+0.56}_{-0.56}$	(4);(48);(50);(4);(52)
970828A	17:44:36.8	RXTE/CGRO/Konus	0.958	147[a]	12.9[a]	$30.4^{+3.6}_{-3.6}$	...	(4);(36);(49);(4)
970508A	21:41:46.8	BeppoSAX/CGRO	0.835	$14.0^{+3.6}_{-3.6}$	$1.70^{+0.31}_{-0.29}$	$0.65^{+0.13}_{-0.13}$	$0.091^{+0.090}_{-0.090}$	(4);(48);(50);(4);(52)
970228A	02:58:01	BeppoSAX/Konus	0.695	$56.0^{+3.2}_{-3.2}$	$1.54^{+0.18}_{-0.19}$	$1.65^{+0.16}_{-0.16}$	$3.1^{+0.2}_{-0.2}$	(4);(48);(50);(4);(6)

References. (1) Pozanenko et al. (2017); (2) Abbott et al. (2017a); (3) Abbott et al. (2017c); (4) Ruffini et al. (2016); (5) Golkhou and Butler (2014); (6) Li et al. (2016); (7) Sang et al. (2016); (8) Jeong et al. (2014); (9) Dichiara et al. (2016); (10) Deng et al. (2016); (11) Cano et al. (2017); (12) Liang et al. (2015); (13) Turpin et al. (2016); (14) Siellez et al. (2016); (15) Racusin et al. (2016); (16) Song et al. (2016); (17) von Kienlin et al. (2014); (18) Margutti et al. (2012); (19) Tunnicliffe et al. (2014); (20) Kopač et al. (2012); (21) Wang et al. (2016); (22) Virgili et al. (2012); (23) Lyman et al. (2017); (24) Sakamoto et al. (2011); (25) Butler et al. (2010); (26) Arcodia et al. (2016); (27) Wang and Dai (2014); (28) Robertson and Ellis (2012); (29) Perley et al. (2016); (30) Qin and Chen (2013); (31) Wei et al. (2014); (32) Butler et al. (2007); (33) Dado and Dar (2016); (34) Cui et al. (2012); (35) Lü and Zhang (2014); (36) Chandra and Frail (2012); (37) Krühler et al. (2015); (38) Troja et al. (2008); (39) Pélangeon et al. (2008); (40) Kopač et al. (2013); (41) Rykoff et al. (2009); (42) Collazzi and Schaefer (2008); (43) Perley et al. (2013); (44) Yonetoku et al. (2010); (45) Minaev et al. (2014); (46) Melandri et al. (2008); (47) Sakamoto et al. (2005); (48) Frontera et al. (2009); (49) Guidorzi et al. (2005); (50) Rossi et al. (2008); (51) Barniol Duran (2014); (52) Bloom et al. (2002); (53) https://gammaray.nsstc.nasa.gov/batse/grb/catalog/current/index.html.

  a   The errors are imputed by MICE algorithm.
  b   The errors in the original papers are in 90% confidence level, we changed the errors to 1 σ confidence level by multiplying 0.995/1.645.
  c   We changed the values into logarithm form or from the logarithm form into the normal form.

Table 4

$L_{\rm pk}$ and the related spectral information. The definition of each parameter is shown in Section 2. The data are selected with accompanied offset available.

GRB	$L_{\rm pk}$ [a] $(10^{52}$ erg s$^{-1})$	$-\alpha$	$-\beta$	$E_{\rm pk}$ (keV)	Model	ref
170817A	$1.6E-5^{+2.5E-5}_{-4E-6}$ [d,f]	...	...	...		(1);(2)
130606A	$8^{+2.8}_{-2.1}$ [c,d]	$1.140^{+0.091}_{-0.091}$ [b]	...	294^{+54}_{-30} [b]	CPL	(3);(4);(4);(4)
130427A	$7.1^{+0.3}_{-0.3}$ [c,d]	$0.91^{+0.01}_{-0.01}$	$3.18^{+0.03}_{-0.03}$	$877.8^{+4.9}_{-4.9}$	Band	(3);(4);(5);(5);(5)
110731A	$8.1^{+1.1}_{-1.1}$ [c,d]	$0.82^{+0.03}_{-0.03}$	$2.32^{+0.03}_{-0.02}$	312^{+29}_{-27} [e]	Band	(3);(4);(6);(6);(6)
100816A	$0.984^{+0.022}_{-0.022}$	...	...	...		(7);(8)
091208B	$2.05^{+0.31}_{-0.41}$	...	...	...		(9);(10)
091127A	$0.358^{+0.015}_{-0.015}$	...	...	...		(9);(4)
090618	$0.937^{+0.012}_{-0.012}$	...	...	...		(7);(4)
090426	$2.90^{+0.78}_{-0.63}$ [c,d]	$1.93^{+0.13}_{-0.13}$ [b]	...	...	SPL	(3);(4);(4)
090424A	$1.680^{+0.029}_{-0.029}$	...	...	...		(7);(4)
090418A	$1.18^{+0.19}_{-0.34}$	...	...	...		(9);(10)
090205A	$1.30^{+1.4}_{-0.94}$ [c,d]	$1.0^{+0.6}_{-1.2}$ [b]	...	33^{+19}_{-19} [b]	CPL	(3);(4);(11);(11)
090102A	$5.83^{+0.84}_{-0.82}$	...	...	...		(9);(4)
081221A	$11.8^{+0.2}_{-0.2}$	...	...	...		(7);(4)
081121A	$5.37^{+0.74}_{-0.74}$	...	...	...		(7);(4)
081008A	$0.55^{+0.14}_{-0.14}$ [c,d]	$1.010^{+0.073}_{-0.073}$ [b]	$2.09^{+0.13}_{-0.13}$ [b]	166^{+22}_{-22} [b]	Band	(3);(4);(12);(12);(12)
081007A	$0.034^{+0.016}_{-0.014}$ [c,d]	$1.40^{+0.36}_{-0.6}$ [b]	...	$27.0^{+6.7}_{-9.7}$ [b]	CPL	(3);(4);(11);(11)
080928	$0.474^{+0.18}_{-0.084}$ [c,d]	$1.70^{+0.06}_{-0.06}$ [b]	...	74^{+147}_{-16} [b]	CPL	(3);(4);(11);(11)
080916A	$0.108^{+0.005}_{-0.005}$	...	...	...		(7);(10)
080805A	$0.211^{+0.11}_{-0.051}$ [c,d]	$1.540^{+0.054}_{-0.054}$ [b]	...	300^{+333}_{-115} [b]	CPL	(3);(4);(11);(11)
080707A	$0.221^{+0.076}_{-0.073}$ [c,d]	$1.78^{+0.17}_{-0.17}$	...	...	SPL	(3);(4);(13)
080607A	129^{+26}_{-26}	...	...	...		(9);(4)
080605A	$9.82^{+0.18}_{-0.18}$	...	...	...		(7);(4)
080430	$0.103^{+0.13}_{-0.007}$	...	...	...		(14);(4)
080319C	$6.04^{+8}_{-0.42}$	...	...	...		(14);(4)
080319B	$7.39^{+0.71}_{-0.71}$	...	...	...		(9);(4)
080207A	$0.61^{+0.11}_{-0.11}$	...	...	...		(7);(4)
071227A	$0.0334^{+0.0049}_{-0.0049}$	...	...	...		(15);(4)
071122	$0.035^{+0.06}_{-0.026}$ [c,d]	$1.60^{+0.24}_{-0.24}$ [b]	...	111^{+318}_{-41} [b]	CPL	(3);(4);(11);(11)
071112C	$4.0^{+1.1}_{-1.1}$ [c,d]	$1.090^{+0.042}_{-0.042}$ [b]	...	...	SPL	(3);(4);(16)
071010A	$1.97^{+0.9}_{-0.78}$ [c,d]	$2.24^{+0.19}_{-0.22}$	...	...	SPL	(3);(10);(4)
071010B	$0.605^{+0.014}_{-0.014}$	...	...	...		(7);(4)
070802A	$0.24^{+0.2}_{-0.14}$ [c,d]	$1.80^{+0.18}_{-0.18}$ [b]	...	55^{+161}_{-21} [b]	CPL	(3);(4);(11);(11)
070724A	$0.0158^{+0.0034}_{-0.0014}$	...	...	...		(15);(4)
070714B	$1.45^{+0.17}_{-0.38}$	...	...	...		(9);(4)
070508	$2.374^{+0.037}_{-0.037}$	...	...	...		(7);(4)
070429B	$0.246^{+0.038}_{-0.038}$	...	...	...		(15);(17)
070318A	$0.073^{+0.048}_{-0.015}$ [c,d]	$1.410^{+0.048}_{-0.048}$ [b]	...	196^{+269}_{-47} [b]	CPL	(3);(4);(18);(18)
070306A	$0.867^{+1.4}_{-0.027}$	...	...	...		(14);(4)
061217	$0.108^{+0.018}_{-0.018}$	...	...	...		(15);(19)
061210A	$0.215^{+0.014}_{-0.014}$	...	...	...		(15);(19)
061110B	$0.59^{+0.94}_{-0.38}$ [c,d]	$0.70^{+0.12}_{-0.12}$ [b]	...	550^{+593}_{-151} [b]	CPL	(3);(4);(18);(18)
061110A	$0.0170^{+0.011}_{-0.0051}$ [c,d]	$1.60^{+0.06}_{-0.06}$ [b]	...	106^{+181}_{-24} [b]	CPL	(3);(4);(18);(18)
061007A	$14.3^{+2.3}_{-1.8}$	...	...	...		(9);(10)
061006A	$0.2460^{+0.012}_{-0.0077}$	...	...	...		(15);(4)
060912A	$1.076^{+0.16}_{-0.095}$ [c]	$5.2^{+1.2}_{-1.2}$	...	200^{+339}_{-67} [b]	CPL	(20);(4);(18);(18)
060801A	$0.476^{+0.062}_{-0.016}$	...	...	...		(15);(17)
060729A	$0.0196^{+0.0085}_{-0.0041}$ [c,d]	$1.80^{+0.06}_{-0.06}$ [b]	...	67^{+139}_{-15} [b]	CPL	(3);(4);(18);(18)
060719A	$0.54^{+0.16}_{-0.15}$ [c,d]	$1.90^{+0.06}_{-0.06}$ [b]	...	55^{+31}_{-31} [b]	CPL	(3);(4);(18);(18)
060614A	$0.00808^{+0.0013}_{-0.00094}$	...	...	...		(9);(4)
060605A	$0.91^{+0.13}_{-0.13}$	...	...	...		(21);(4)
060602A	$0.061^{+0.025}_{-0.008}$	...	...	...		(15);(10)
060522	$2.33^{+0.78}_{-0.81}$	...	...	...		(9);(4)
060502B	0.0065^{+9E-4}_{-9E-4}	...	...	...		(15);(19)
060418A	$1.96^{+0.43}_{-0.13}$	...	...	...		(14);(4)
060218A	$4.3E-6^{+1.5E-6}_{-1.7E-6}$	...	...	...		(9);(4)
060206A	$7.18^{+0.27}_{-0.27}$	...	...	...		(7);(4)
060124A	$10.2^{+3.1}_{-2.9}$	...	...	...		(9);(4)
060121A	$24.5^{+1.6}_{-1.6}$	...	...	...		(15);(4)
060115A	$1.55^{+0.13}_{-0.13}$	...	...	...		(7);(4)
051221A	$0.258^{+0.009}_{-0.009}$	...	...	...		(15);(4)

Table 4 (*continued*)

GRB	L_{pk}[a] $(10^{52}$ erg s$^{-1})$	$-\alpha$	$-\beta$	E_{pk} (keV)	Model	ref
051022A	$3.12^{+0.41}_{-0.41}$	...	...	...		(9);(4)
051016B	$0.065^{+0.048}_{-0.038}$	...	...	...		(9);(4)
050904A	$8.5^{+2.3}_{-2.4}$	...	...	...		(9);(4)
050826A	$0.0033^{+0.0032}_{-8E-4}$	...	...	...		(15);(4)
050824A	$0.18^{+0.19}_{-0.17}$[c,d]	$2.76^{+0.23}_{-0.23}$[b]	...	...	SPL	(3);(4);(4)
050820A	$3.22^{+0.3}_{-0.45}$	...	...	...		(9);(4)
050813	$0.04^{+0.02}_{-0.02}$	...	...	...		(15);(17)
050724A	$0.0099^{+0.0023}_{-0.001}$	...	...	...		(15);(4)
050709A	$0.0540^{+0.0067}_{-0.0069}$	...	...	...		(15);(4)
050525A	$1.159^{+0.016}_{-0.016}$	...	...	...		(7);(4)
050509B	$7E-4^{+0.001}_{-5E-4}$	...	...	...		(15);(4)
050416A	$0.087^{+0.019}_{-0.015}$	...	...	...		(9);(4)
050401A	$12.0^{+2.3}_{-2.6}$	...	...	...		(9);(4)
050315	$0.88^{+0.33}_{-0.31}$	...	...	...		(9);(4)
041006A	$0.531^{+0.022}_{-0.022}$	...	...	...		(9);(4)
040924A	$0.86^{+0.09}_{-0.09}$	...	...	...		(9);(4)
030429A	$0.75^{+0.19}_{-0.22}$	...	...	...		(9);(4)
030323A	$1.14^{+0.61}_{-0.51}$	...	...	...		(9);(4)
021004A	$0.91^{+0.19}_{-0.19}$	...	...	...		(9);(4)
010921A	$0.13^{+0.01}_{-0.01}$	...	...	...		(21);(4)
010222A	$28.7^{+1.3}_{-1.2}$	...	...	...		(9);(4)
000210A	$7.0^{+2.8}_{-1.8}$	...	...	...		(9);(4)
991208A	$4.68^{+1.2}_{-0.83}$	...	...	...		(9);(4)
990705A	$2.21^{+0.19}_{-0.17}$	...	...	...		(9);(4)
990510A	$5.2^{+1.1}_{-1.4}$	...	...	...		(9);(4)
990123A	$27.5^{+1.2}_{-1.2}$	...	...	...		(9);(4)
980703A	$1.20^{+0.13}_{-0.23}$	...	...	...		(9);(4)
980613A	$0.193^{+0.068}_{-0.057}$	...	...	...		(9);(4)
971214B	$9.5^{+5.3}_{-4}$	...	...	...		(9);(22)
970508A	$0.164^{+0.021}_{-0.021}$	...	...	...		(9);(22)
970228A	$1.54^{+0.21}_{-0.12}$	...	...	...		(9);(4)

References. (1) Zhang et al. (2017a); (2) Abbott et al. (2017c); (3) Deng et al. (2016); (4) Li et al. (2016); (5) Goldstein et al. (2016); (6) Ackermann et al. (2013); (7) Lin et al. (2016); (8) Kopač et al. (2012); (9) Yonetoku et al. (2010); (10) Lyman et al. (2017); (11) Butler et al. (2010); (12) Heussaff et al. (2013); (13) Krimm et al. (2009); (14) Ukwatta et al. (2010); (15) Zhang et al. (2009); (16) Nava et al. (2012); (17) Tunnicliffe et al. (2014); (18) Butler et al. (2007); (19) Cui et al. (2012); (20) Rizzuto et al. (2007); (21) Rossi et al. (2008); (22) Bloom et al. (2002).

[a] The peak luminosity is for 1 s time binned light curve.
[b] The errors in the original papers are in 90% confidence level, we changed the errors to 1 σ confidence level by multiplying 0.995/1.645.
[c] The values are calculated using the spectral values in order to change the energy band.
[d] We changed the values into logarithm or from logarithm into the normal form.
[e] The values are calculated using α and break energy E_0.
[f] The peak luminosity of GRB 170817A is derived from 50 ms time resolution light curve.

Fig. 1 also gives a clear indication that all the GRBs are gathered in two distinct groups. We apply K-Means clustering algorithms to get the boundary between this two traditionally classes. The boundary is represented with a dash line in Fig. 1. Two different clusters cannot have any object in common. The similarity measure between the cases defined as the euclidean distance on the duration-offset plane. Variables with incompatible units are faced in our dataset. We use logarithmic variables, rather than normalized or standardized variables. Because units can be removed by taking logarithms and the ranges of variables is similar. We kept information on burst duration and offset. The boundaries are $\log(\text{offset}) = 2.33 \times \log T_{90,i} - 0.63$ and $\log(\text{offset}) = 1.73 \times \log T_{R45,i} + 0.92$. We assume that the group of bursts on the duration-offset plane is separated and equal-sized. Each cluster is described by a single point known as the centroid. The centroid of each class is defined as the mean values of $\log T_{90,i}$, $\log T_{R45,i}$, and $\log(\text{offset})$. The centroids are marked with black open triangles in Fig. 1. These two groups are generally consistent with long and short GRBs, while with few outliers.

We have also checked the correlations of the offset with other parameters, while no much significant relations has been found. For the offset $- E_p$ correlation, as the peak energy can be best fit with Band function or with CPL model, there are two correlations. For the Band function model, the Pearson coefficient is 0.30 ± 0.22 with p-value 0.32. For the CPL model, the Pearson coefficient is 0.03 ± 0.13 with p-value 0.88. Though there is relatively weak correlation between offset and L_{pk}, there is no strong evidence for offset and $L_{\gamma,iso}$. The corresponding Pearson coefficient is $-0.03^{+0.01}_{-0.03}$ with p-value 0.73 as also shown in Table 2.

It is important to decide the true number of groups. There is no certain way of telling the goodness of the clustering. The silhouette coefficient is a measure of the compactness and separation of the clusters. It increases as the quality of the clusters increase, it is large for compact clusters that are far from each other and small for large and overlapping clusters. According to the silhouette coefficient, the most probable number of clusters is 2 for our set of GRBs.

To figure out the correlations are solely caused by the long or short GRBs progenitors, or there is intrinsic tendency inside LGRBs or SGRBs, we divided the 304 GRBs into SGRBs and LGRBs following the widely believed relation of T_{90} with 2 s. The coefficients are also listed in the Table 2. We list the relations with mean correlation coefficient p-value smaller than 0.1.

The relation between $E_{\gamma,\text{iso}}$ and host galaxy offsets for SGRBs is:

$$\log(\text{offset}) = -0.22^{+0.02}_{-0.05} \times \log E_{\gamma,\text{iso},52} + 0.71^{+0.05}_{-0.05}, \qquad (9)$$

where the offset is in unit of kpc, and $E_{\gamma,\text{iso},52}$ is in unit of 10^{52} ergs.

The relation between L_{pk} and host galaxy offsets for SGRBs is:

$$\log(\text{offset}) = -0.49^{+0.04}_{-0.08} \times \log L_{\text{pk},52} + 0.35^{+0.13}_{-0.13}, \qquad (10)$$

where the offset is in unit of kpc, and $L_{\text{pk},52}$ is in unit of 10^{52} erg/s.

The relation between $T_{\text{R45,i}}$ and $E_{\gamma,\text{iso}}$ for SGRBs is:

$$\log E_{\gamma,\text{iso},52} = 1.45^{+0.05}_{-0.11} \times \log T_{\text{R45,i}} + 0.5^{+0.12}_{-0.12}, \qquad (11)$$

where $T_{\text{R45,i}}$ are in units of seconds, and $E_{\gamma,\text{iso},52}$ is in unit of 10^{52} ergs.

The relation between $T_{\text{R45,i}}$ and $E_{\gamma,\text{iso}}$ for LGRBs is:

$$\log E_{\gamma,\text{iso},52} = 0.36^{+0.01}_{-0.02} \times \log T_{\text{R45,i}} + 0.55^{+0.01}_{-0.01}, \qquad (12)$$

where $T_{\text{R45,i}}$ are in units of seconds, and $E_{\gamma,\text{iso},52}$ is in unit of 10^{52} ergs.

When the GRBs are divided into long and short ones, there is no clear correlation between the offset and the duration. It shows that the origin of LGRBs and SGRBs is only due to the spatial offset. The correlations of $\log(\text{offset}) - \log E_{\gamma,\text{iso}}$ and $\log(\text{offset}) - \log L_{\text{pk}}$ observed only for SGRBs. It might indicate that the SGRBs can still be divided into several sub-groups. A possible explanation could be the sub-groups of NS–NS merging and BH–NS merging as origin of SGRBs. For the BH–NS merger, the total gravitational energy is larger than the NS–NS merger, as the BH mass can be much larger. On the other hand, the more massive BH is harder to be kicked outside the host galaxy, and should be located near to the center. This naturally explains the anti-correlation shown in Eq. (9). Interestingly, as shown in Table 2 for short GRBs, also for the offset $- L_{\gamma,\text{iso}}$ and offset $- L_{\text{pk}}$, one is quite weak (Pearson coefficient being $0.07^{+0.07}_{-0.04}$ with p-value 0.19 for offset $-L_{\gamma,\text{iso}}$) while the other is relatively quite strong (Pearson coefficient being $-0.62^{+0.03}_{-0.06}$ with p-value 0.02 for offset $- L_{\text{pk}}$).

Interestingly, the $E_{\gamma,\text{iso}} - T_{\text{R45,i}}$ relation has also been observed, however the coefficients are quite different for the combined GRBs, SGRBs and LGRBs, as shown in Table 2 and in Eqs. (8) and (12). Especially, for the combine sample and for Short GRBs alone, the Pearson coefficients are $0.425^{+0.003}_{-0.007}$ with p-value 3.6×10^{-14} and $0.53^{+0.01}_{-0.04}$ with p-value 0.01. These relations are quite strong. However, the underlying reason is not clear.

4. Conclusion and discussion

In this work, we studied the relations of the spatial position of GRBs in their host galaxies with their durations and energies. Using the available data, we tested the correlations between $T_{90,\text{i}}$, $T_{\text{R45,i}}$, $E_{\gamma,\text{iso}}$, $L_{\gamma,\text{iso}}$, L_{pk} and corresponding spatial offset in their host galaxies. We found the host galaxy offsets have negative correlations with the other four parameters. This negative relation for ($T_{90,\text{i}}$ and $T_{\text{R45,i}}$) seems reasonable, because LGRBs are most-likely from massive star collapsing, so the GRB positions are closer to the center of its host galaxies. On the other hand, SGRBs are most-likely from binary mergers. For the binary mergers, the system will experience large velocity kicks at birth, leading to eventual mergers outside the host galaxies (Berger, 2010). Therefore, mostly SGRBs have bigger spatial offsets than LGRBs. But there is no correlation about host galaxy offsets and duration for SGRBs and LGRBs respectively, so different origins offer a natural explanation for the two negative correlations. Interestingly, L_{pk} is related to the offset,

while $L_{\gamma,\text{iso}}$ is not, and the $E_{\gamma,\text{iso}} - T_{\text{R45,i}}$ relation is quite different of the long GRBs, short GRBs and the combined sample. We also found the special GRBs 170817A and 060218A are outliers in most of the scatter plots, which might indicate there are more sub-groups in the GRB samples.

Considering the relation between the $E_{\gamma,\text{iso}}$ and the offsets, for the combined GRBs analysis, as the SGRBs have lower energy than LGRBs, it becomes natural that $E_{\gamma,\text{iso}}$ and the host galaxy offsets have negative correlation. We have found a similar correlation for SGRBs. We interpret it as a result of different progenitors. If the progenitor is NS–BH, the SGRBs have larger $E_{\gamma,\text{iso}}$ and smaller spatial offset, because the bigger mass of the system and smaller kick velocity. While for the NS–NS progenitors, the behaviors are on the opposite. For the positive correlation of $E_{\gamma,\text{iso}}$ and $T_{\text{R45,i}}$, we can find significant correlation for the combined GRBs, SGRBs and LGRBs. Therefore, it is a common property for GRBs, no matter what the central engines or progenitors are.

We have seen the main tendency is that: for SGRBs, they are distributed in the outer side of the host galaxies, while for the LGRBs, they are in the inner side. This supports again that the SGRBs are from mergers of compact stars (NS–NS, or NS–BH), while the LGRBs are from the core collapsing of the massive stars. With this topic, the strongest evidence is the SNe Ic connection to the long GRBs, such as GRB 980425/SN 1998bw (Galama et al., 1998), while for the short GRBs is the gravitational wave event association, i.e., the most recently discovered NS–NS merger event GRB 170817A/GW170817 (Abbott et al., 2017b). Within the SGRBs, it also shows an anti-correlation between the offset and isotropic γ-ray energy. This may indicate the double origins for the SGRBs, i.e., NS–NS origin with lower energy and locating nearer the center of the host galaxy, while BH–NS origin with higher energy and locating at outer side. A possible explanation might be that at the birth of the NS or BH, for very high speed NS, the companion compact star has the chance to decouple, while the high speed BH (with more mass) binary can survive, and consequently reaches to outer area of the host galaxy. Also because of the range of the BH masses, it may explain the variety of the magnitude of the kilonovae (or called macronovae, merger novae) (Gao et al., 2017). We have analyzed the correlations by dividing the sample into long GRBs and short GRBs based on the duration being greater or smaller than 2 s. It is also possible to perform the same analysis based on the k-means classification, which were given in Section 3. As one can see, the sample does not change much, and the results may not change much neither.

Our data is biased for strong or optically bright GRBs. The optically dark GRBs are hard to identify the host galaxies and hence the spatial offsets are not available. The GRBs can be dark due to high absorption by the dense medium which may not affect the biasing of offset. In the case intrinsically dark GRBs, the offset might be intrinsically different from the bright GRBs. However to investigate the answer to this property is beyond the scope of this work. It is possible that the GRB location is just occasionally overlapping with a galaxy, while the host galaxy is much dimmer in the foreground or background. This may introduce some bias to the data, especially for the large offset ones. Additionally, our statistical analysis totally rely on observational resolution and technology.

In the future, one can get more information about the host galaxy with the enhancement of the GRB monitors and observations with higher angular resolution. Monitoring the host galaxies mostly rely on the ground optical follow up efficiency. With more powerful telescope, one can get more information on-site the position of the GRB location (not only the whole galaxy). The environment, such as circum-burst density, star formation rate etc., are also important observations to be made. These information are crucial for understanding the physics of GRBs as well as the final stage of the stellar evolution.

Acknowledgments

References

Abbott, B.P., Abbott, R., Abbott, T.D., Acernese, F., Ackley, K., Adams, C., Adams, T., Addesso, P., Adhikari, R.X., Adya, V.B., et al., 2017a. Gravitational waves and gamma-rays from a binary neutron star merger: GW170817 and GRB 170817A. Astrophys. J. 848, L13.

Abbott, B.P., Abbott, R., Abbott, T.D., Acernese, F., Ackley, K., Adams, C., Adams, T., Addesso, P., Adhikari, R.X., Adya, V.B., et al., 2017b. Multi-messenger observations of a binary neutron star merger. Astrophys. J. 848, L12.

Abbott, B.P., Abbott, R., Abbott, T.D., Acernese, F., Ackley, K., Adams, C., Adams, T., Addesso, P., Adhikari, R.X., Adya, V.B., et al., 2017c. On the progenitor of binary neutron star merger GW170817. Astrophys. J. 850, L40.

Ackermann, M., Ajello, M., Asano, K., Axelsson, M., Baldini, L., Ballet, J., Barbiellini, G., Bastieri, D., Bechtol, K., Bellazzini, R., Bhat, P.N., Bissaldi, E., Bloom, E.D., Bonamente, E., Bonnell, J., Bouvier, A., Brandt, T.J., Bregeon, J., Brigida, M., Bruel, P., Buehler, R., Burgess, J.M., Buson, S., Byrne, D., Caliandro, G.A., Cameron, R.A., Caraveo, P.A., Cecchi, C., Charles, E., Chaves, R.C.G., Chekhtman, A., Chiang, J., Chiaro, G., Ciprini, S., Claus, R., Cohen-Tanugi, J., Connaughton, V., Conrad, J., Cutini, S., D'Ammando, F., de Angelis, A., de Palma, F., Dermer, C.D., Desiante, R., Digel, S.W., Dingus, B.L., Di Venere, L., Drell, P.S., Drlica-Wagner, A., Dubois, R., Favuzzi, C., Ferrara, E.C., Fitzpatrick, G., Foley, S., Franckowiak, A., Fukazawa, Y., Fusco, P., Gargano, F., Gasparrini, D., Gehrels, N., Germani, S., Giglietto, N., Giommi, P., Giordano, F., Giroletti, M., Glanzman, T., Godfrey, G., Goldstein, A., Granot, J., Grenier, I.A., Grove, J.E., Gruber, D., Guiriec, S., Hadasch, D., Hanabata, Y., Hayashida, M., Horan, D., Hou, X., Hughes, R.E., Inoue, Y., Jackson, M.S., Jogler, T., Jóhannesson, G., Johnson, A.S., Johnson, W.N., Kamae, T., Kataoka, J., Kawano, T., Kippen, R.M., Knödlseder, J., Kocevski, D., Kouveliotou, C., Kuss, M., Lande, J., Larsson, S., Latronico, L., Lee, S.-H., Longo, F., Loparco, F., Lovellette, M.N., Lubrano, P., Massaro, F., Mayer, M., Mazziotta, M.N., McBreen, S., McEnery, J.E., McGlynn, S., Michelson, P.F., Mizuno, T., Moiseev, A.A., Monte, C., Monzani, M.E., Moretti, E., Morselli, A., Murgia, S., Nemmen, R., Nuss, E., Nymark, T., Ohno, M., Ohsugi, T., Omodei, N., Orienti, M., Orlando, E., Paciesas, W.S., Paneque, D., Panetta, J.H., Pelassa, V., Perkins, J.S., Pesce-Rollins, M., Piron, F., Pivato, G., Porter, T.A., Preece, R., Racusin, J.L., Rainò, S., Rando, R., Rau, A., Razzano, M., Razzaque, S., Reimer, A., Reimer, O., Reposeur, T., Ritz, S., Romoli, C., Roth, M., Ryde, F., Saz Parkinson, P.M., Schalk, T.L., Sgrò, C., Siskind, E.J., Sonbas, E., Spandre, G., Spinelli, P., Suson, D.J., Tajima, H., Takahashi, H., Takeuchi, Y., Tanaka, Y., Thayer, J.G., Thayer, J.B., Thompson, D.J., Tibaldo, L., Tierney, D., Tinivella, M., Torres, D.F., Tosti, G., Troja, E., Tronconi, V., Usher, T.L., Vandenbroucke, J., van der Horst, A.J., Vasileiou, V., Vianello, G., Vitale, V., von Kienlin, A., Winer, B.L., Wood, K.S., Wood, M., Xiong, S., Yang, Z., 2013. The first Fermi-LAT gamma-ray burst catalog. Astrophys. J. Suppl. Ser. 209, 11.

Arcodia, R., Campana, S., Salvaterra, R., 2016. The dependence of gamma-ray burst X-ray column densities on the model for Galactic hydrogen. Astron. Astrophys. 590, A82.

Barniol Duran, R., 2014. Constraining the magnetic field in GRB relativistic collisionless shocks using radio data. Mon. Not. R. Astron. Soc. 442, 3147–3154.

Berger, E., 2010. A short gamma-ray burst "no-host" problem? Investigating large progenitor offsets for short GRBs with optical afterglows. Astrophys. J. 722, 1946–1961.

Bloom, J.S., Kulkarni, S.R., Djorgovski, S.G., 2002. The observed offset distribution of gamma-ray bursts from their host galaxies: a robust clue to the nature of the progenitors. Astron. J. 123, 1111–1148.

Butler, N.R., Bloom, J.S., Poznanski, D., 2010. The cosmic rate, luminosity function, and intrinsic correlations of long gamma-ray bursts. Astrophys. J. 711, 495–516.

Butler, N.R., Kocevski, D., Bloom, J.S., Curtis, J.L., 2007. A complete catalog of Swift gamma-ray burst spectra and durations: demise of a physical origin for pre-Swift high-energy correlations. Astrophys. J. 671, 656–677.

Cano, Z., Wang, S.-Q., Dai, Z.-G., Wu, X.-F., 2017. The observer's guide to the gamma-ray burst supernova connection. Adv. Astron. 2017, 8929054.

Chandra, P., Frail, D.A., 2012. A radio-selected sample of gamma-ray burst afterglows. Astrophys. J. 746, 156.

Church, R.P., Levan, A.J., Davies, M.B., Tanvir, N., 2011. Implications for the origin of short gamma-ray bursts from their observed positions around their host galaxies. Mon. Not. R. Astron. Soc. 413, 2004–2014.

Collazzi, A.C., Schaefer, B.E., 2008. Does the addition of a duration improve the L_{iso}-E_{peak} relation for gamma-ray bursts? Astrophys. J. 688, 456–461.

Cui, X.-H., Nagataki, S., Aoi, J., Xu, R.-X., 2012. Origins of short gamma-ray bursts deduced from offsets in their host galaxies revisited. Res. Astron. Astrophys. 12 (9), 1255. http://stacks.iop.org/1674-4527/12/i=9/a=006.

Dado, S., Dar, A., 2016. Critical test of gamma-ray burst theories. Phys. Rev. D 94 (6), 063007.

Deng, C.-M., Wang, X.-G., Guo, B.-B., Lu, R.-J., Wang, Y.-Z., Wei, J.-J., Wu, X.-F., Liang, E.-W., 2016. Cosmic evolution of long gamma-ray burst luminosity. Astrophys. J. 820, 66.

Dichiara, S., Guidorzi, C., Amati, L., Frontera, F., Margutti, R., 2016. Correlation between peak energy and Fourier power density spectrum slope in gamma-ray bursts. Astron. Astrophys. 589, A97.

Eichler, D., Livio, M., Piran, T., Schramm, D.N., 1989. Nucleosynthesis, neutrino bursts and gamma-rays from coalescing neutron stars. Nature 340, 126–128.

Feigelson, E.D., Babu, G.J., 2012. Modern Statistical Methods for Astronomy.

Fong, W., Berger, E., Fox, D.B., 2010. Hubble space telescope observations of short gamma-ray burst host galaxies: morphologies, offsets, and local environments. Astrophys. J. 708, 9–25.

Fong, W., Berger, E., Margutti, R., Zauderer, B.A., 2015. A decade of short-duration gamma-ray burst broadband afterglows: energetics, circumburst densities, and jet opening angles. Astrophys. J. 815, 102.

Frontera, F., Guidorzi, C., Montanari, E., Rossi, F., Costa, E., Feroci, M., Calura, F., Rapisarda, M., Amati, L., Carturan, D., Cinti, M.R., Fiume, D.D., Nicastro, L., Orlandini, M., 2009. The gamma-ray burst catalog obtained with the gamma-ray burst monitor aboard BeppoSAX. Astrophys. J. Suppl. Ser. 180, 192–223.

Galama, T.J., Vreeswijk, P.M., van Paradijs, J., Kouveliotou, C., Augusteijn, T., Böhnhardt, H., Brewer, J.P., Doublier, V., Gonzalez, J.-F., Leibundgut, B., Lidman, C., Hainaut, O.R., Patat, F., Heise, J., in't Zand, J., Hurley, K., Groot, P.J., Strom, R.G., Mazzali, P.A., Iwamoto, K., Nomoto, K., Umeda, H., Nakamura, T., Young, T.R., Suzuki, T., Shigeyama, T., Koshut, T., Kippen, M., Robinson, C., de Wildt, P., Wijers, R.A.M.J., Tanvir, N., Greiner, J., Pian, E., Palazzi, E., Frontera, F., Masetti, N., Nicastro, L., Feroci, M., Costa, E., Piro, L., Peterson, B.A., Tinney, C., Boyle, B., Cannon, R., Stathakis, R., Sadler, E., Begam, M.C., Ianna, P., 1998. An unusual supernova in the error box of the γ-ray burst of 25 April 1998. Nature 395, 670–672.

Gao, H., Zhang, B., Lü, H.-J., Li, Y., 2017. Searching for magnetar-powered mergernovae from short GRBS. Astrophys. J. 837, 50.

Goldstein, A., Connaughton, V., Briggs, M.S., Burns, E., 2016. Estimating Long GRB Jet Opening Angles and Rest-Frame Energetics. AAS/High Energy Astrophysics Division, vol. 15. AAS/High Energy Astrophysics Division. p. 306.07.

Golkhou, V.Z., Butler, N.R., 2014. Uncovering the Intrinsic Variability of Gamma-Ray Bursts. AAS/High Energy Astrophysics Division, vol. 14. AAS/High Energy Astrophysics Division. p. 112.04.

Guidorzi, C., Frontera, F., Montanari, E., Rossi, F., Amati, L., Gomboc, A., Hurley, K., Mundell, C.G., 2005. The gamma-ray burst variability-peak luminosity correlation: new results. Mon. Not. R. Astron. Soc. 363, 315–325.

Heussaff, V., Atteia, J.-L., Zolnierowski, Y., 2013. The E_{peak}-E_{iso} relation revisited with Fermi GRBs. Resolving a long-standing debate? Astron. Astrophys. 557, A100.

Jeong, S., Castro-Tirado, A.J., Bremer, M., Winters, J.M., Gorosabel, J., Guziy, S., Pandey, S.B., Jelínek, M., Sánchez-Ramírez, R., Sokolov, I.V., Orekhova, N.V., Moskvitin, A.S., Tello, J.C., Cunniffe, R., Lara-Gil, O., Oates, S.R., Pérez-Ramírez, D., Bai, J., Fan, Y., Wang, C., Park, I.H., 2014. The dark nature of GRB 130528A and its host galaxy. Astron. Astrophys. 569, A93.

Kopač, D., D'Avanzo, P., Melandri, A., Campana, S., Gomboc, A., Japelj, J., Bernardini, M.G., Covino, S., Vergani, S.D., Salvaterra, R., Tagliaferri, G., 2012. On the environment of short gamma-ray bursts. Mon. Not. R. Astron. Soc. 424, 2392–2399.

Kopač, D., Kobayashi, S., Gomboc, A., Japelj, J., Mundell, C.G., Guidorzi, C., Melandri, A., Bersier, D., Cano, Z., Smith, R.J., Steele, I.A., Virgili, F.J., 2013. GRB 090727 and gamma-ray bursts with early-time optical emission. Astrophys. J. 772, 73.

Kouveliotou, C., Meegan, C.A., Fishman, G.J., Bhat, N.P., Briggs, M.S., Koshut, T.M., Paciesas, W.S., Pendleton, G.N., 1993. Identification of two classes of gamma-ray bursts. Astrophys. J. 413, L101–L104.

Krimm, H.A., Yamaoka, K., Sugita, S., Ohno, M., Sakamoto, T., Barthelmy, S.D., Gehrels, N., Hara, R., Norris, J.P., Ohmori, N., Onda, K., Sato, G., Tanaka, H., Tashiro, M., Yamauchi, M., 2009. Testing the E_{peak}-E_{iso} relation for GRBs detected by Swift and Suzaku-WAM. Astrophys. J. 704, 1405–1432.

Krühler, T., Malesani, D., Fynbo, J.P.U., Hartoog, O.E., Hjorth, J., Jakobsson, P., Perley, D.A., Rossi, A., Schady, P., Schulze, S., Tanvir, N.R., Vergani, S.D., Wiersema, K., Afonso, P.M.J., Bolmer, J., Cano, Z., Covino, S., D'Elia, V., de Ugarte Postigo, A., Filgas, R., Friis, M., Graham, J.F., Greiner, J., Goldoni, P., Gomboc, A., Hammer, F., Japelj, J., Kann, D.A., Kaper, L., Klose, S., Levan, A.J., Leloudas, G., Milvang-Jensen, B., Nicuesa Guelbenzu, A., Palazzi, E., Pian, E., Piranomonte, S., Sánchez-Ramírez, R., Savaglio, S., Selsing, J., Tagliaferri, G., Vreeswijk, P.M., Watson, D.J., Xu, D., 2015. GRB hosts through cosmic time. VLT/X-Shooter emission-line spectroscopy of 96 γ-ray-burst-selected galaxies at $0.1 < z < 3.6$. Astron. Astrophys. 581, A125.

Li, Y., Zhang, B., Lü, H.-J., 2016. A comparative study of long and short GRBs. I. Overlapping properties. Astrophys. J. Suppl. Ser. 227, 7.

Liang, E.-W., Lin, T.-T., Lü, J., Lu, R.-J., Zhang, J., Zhang, B., 2015. A tight L_{iso}-$E_{p,z}$-Gamma$_0$ correlation of gamma-ray bursts. Astrophys. J. 813, 116.

Lin, H.-N., Li, X., Chang, Z., 2016. Effect of gamma-ray burst (GRB) spectra on the empirical luminosity correlations and the GRB Hubble diagram. Mon. Not. R. Astron. Soc. 459, 2501–2512.

Little, R.J.A., 1988. Missing-data adjustments in large surveys (c/r: p296-301). J. Bus. Econ. Stat. 6, 287–296.

Lü, H.-J., Zhang, B., 2014. A test of the millisecond magnetar central engine model of gamma-ray bursts with Swift data. Astrophys. J. 785, 74.

Lyman, J.D., Levan, A.J., Tanvir, N.R., Fynbo, J.P.U., McGuire, J.T.W., Perley, D.A., Angus, C.R., Bloom, J.S., Conselice, C.J., Fruchter, A.S., Hjorth, J., Jakobsson, P., Starling, R.L.C., 2017. The host galaxies and explosion sites of long-duration gamma ray bursts: Hubble Space Telescope near-infrared imaging. Mon. Not. R. Astron. Soc. 467, 1795–1817.

MacFadyen, A.I., Woosley, S.E., 1999. Collapsars: gamma-ray bursts and explosions in "failed supernovae". Astrophys. J. 524, 262–289.

Malesani, D., Covino, S., D'Avanzo, P., D'Elia, V., Fugazza, D., Piranomonte, S., Ballo, L., Campana, S., Stella, L., Tagliaferri, G., Antonelli, L.A., Chincarini, G., Della Valle, M., Goldoni, P., Guidorzi, C., Israel, G.L., Lazzati, D., Melandri, A., Pellizza, L.J., Romano, P., Stratta, G., Vergani, S.D., 2007. Multicolor observations of the afterglow of the short/hard GRB 050724. Astron. Astrophys. 473, 77–84.

Margutti, R., Berger, E., Fong, W., Zauderer, B.A., Cenko, S.B., Greiner, J., Soderberg, A.M., Cucchiara, A., Rossi, A., Klose, S., Schmidl, S., Milisavljevic, D., Sanders, N., 2012. The afterglow and environment of the short GRB 111117A. Astrophys. J. 756, 63.

Melandri, A., Mundell, C.G., Kobayashi, S., Guidorzi, C., Gomboc, A., Steele, I.A., Smith, R.J., Bersier, D., Mottram, C.J., Carter, D., Bode, M.F., O'Brien, P.T., Tanvir, N.R., Rol, E., Chapman, R., 2008. The early-time optical properties of gamma-ray burst afterglows. Astrophys. J. 686, 1209–1230.

Minaev, P.Y., Pozanenko, A.S., Molkov, S.V., Grebenev, S.A., 2014. Catalog of short gamma-ray transients detected in the SPI/INTEGRAL experiment. Astron. Lett. 40, 235–267.

Narayan, R., Paczynski, B., Piran, T., 1992. Gamma-ray bursts as the death throes of massive binary stars. Astrophys. J. 395, L83–L86.

Nava, L., Salvaterra, R., Ghirlanda, G., Ghisellini, G., Campana, S., Covino, S., Cusumano, G., D'Avanzo, P., D'Elia, V., Fugazza, D., Melandri, A., Sbarufatti, B., Vergani, S.D., Tagliaferri, G., 2012. A complete sample of bright Swift long gamma-ray bursts: testing the spectral-energy correlations. Mon. Not. R. Astron. Soc. 421, 1256–1264.

Paczynski, B., 1991. Cosmological gamma-ray bursts. Acta Astron. 41, 257–267.

Pélangeon, A., Atteia, J.-L., Nakagawa, Y.E., Hurley, K., Yoshida, A., Vanderspek, R., Suzuki, M., Kawai, N., Pizzichini, G., Boër, M., Braga, J., Crew, G., Donaghy, T.Q., Dezalay, J.P., Doty, J., Fenimore, E.E., Galassi, M., Graziani, C., Jernigan, J.G., Lamb, D.Q., Levine, A., Manchanda, J., Martel, F., Matsuoka, M., Olive, J.-F., Prigozhin, G., Ricker, G.R., Sakamoto, T., Shirasaki, Y., Sugita, S., Takagishi, K., Tamagawa, T., Villasenor, J., Woosley, S.E., Yamauchi, M., 2008. Intrinsic properties of a complete sample of HETE-2 gamma-ray bursts. A measure of the GRB rate in the Local Universe. Astron. Astrophys. 491, 157–171.

Perley, D.A., Levan, A.J., Tanvir, N.R., Cenko, S.B., Bloom, J.S., Hjorth, J., Krühler, T., Filippenko, A.V., Fruchter, A., Fynbo, J.P.U., Jakobsson, P., Kalirai, J., Milvang-Jensen, B., Morgan, A.N., Prochaska, J.X., Silverman, J.M., 2013. A population of massive, luminous galaxies hosting heavily dust-obscured gamma-ray bursts: implications for the use of GRBs as tracers of cosmic star formation. Astrophys. J. 778, 128.

Perley, D.A., Tanvir, N.R., Hjorth, J., Laskar, T., Berger, E., Chary, R., de Ugarte Postigo, A., Fynbo, J.P.U., Krühler, T., Levan, A.J., Michałowski, M.J., Schulze, S., 2016. The Swift GRB Host Galaxy Legacy Survey. II. Rest-frame near-IR luminosity distribution and evidence for a near-solar metallicity threshold. Astrophys. J. 817, 8.

Pozanenko, A., Barkov, M.V., Minaev, P.Y., Volnova, A.A., Mazaeva, E.D., Moskvitin, A.S., Krugov, M.A., Samodurov, V.A., Loznikov, V.M., Lyutikov, M., 2017. GRB170817A associated with GW170817: multifrequency observations and modeling of prompt gamma-ray emission. ArXiv e-prints.

Qin, Y.-P., Chen, Z.-F., 2013. Statistical classification of gamma-ray bursts based on the Amati relation. Mon. Not. R. Astron. Soc. 430, 163–173.

Racusin, J.L., Oates, S.R., de Pasquale, M., Kocevski, D., 2016. A correlation between the intrinsic brightness and average decay rate of gamma-ray burst X-ray afterglow light curves. Astrophys. J. 826, 45.

Reichart, D.E., Lamb, D.Q., Fenimore, E.E., Ramirez-Ruiz, E., Cline, T.L., Hurley, K., 2001. A possible Cepheid-like luminosity estimator for the long gamma-ray bursts. Astrophys. J. 552, 57–71.

Rizzuto, D., Guidorzi, C., Romano, P., Covino, S., Campana, S., Capalbi, M., Chincarini, G., Cusumano, G., Fugazza, D., Mangano, V., Moretti, A., Perri, M., Tagliaferri, G., 2007. Testing the gamma-ray burst variability/peak luminosity correlation on a Swift homogeneous sample. Mon. Not. R. Astron. Soc. 379, 619–628.

Robertson, B.E., Ellis, R.S., 2012. Connecting the gamma ray burst rate and the cosmic star formation history: implications for reionization and galaxy evolution. Astrophys. J. 744, 95.

Rossi, F., Guidorzi, C., Amati, L., Frontera, F., Romano, P., Campana, S., Chincarini, G., Montanari, E., Moretti, A., Tagliaferri, G., 2008. Testing the $E_{p,i}$-$L_{p,iso}$-$T_{0.45}$ correlation on a BeppoSAX and Swift sample of gamma-ray bursts. Mon. Not. R. Astron. Soc. 388, 1284–1292.

Rubin, D.B., 1976. Inference and missing data. Biometrika 63, 581–590.

Rubin, D.B., 1987. Multiple Imputation For Nonresponse in Surveys. John Wiley and Sons, New York.

Rubin, D.B., 1996. Multiple imputation after 18+ years. J. Am. Stat. Assoc. 91 (434), 473–489. http://www.jstor.org/stable/2291635.

Ruffini, R., Rueda, J.A., Muccino, M., Aimuratov, Y., Becerra, L.M., Bianco, C.L., Kovacevic, M., Moradi, R., Oliveira, F.G., Pisani, G.B., Wang, Y., 2016. On the classification of GRBs and their occurrence rates. Astrophys. J. 832, 136.

Rykoff, E.S., Aharonian, F., Akerlof, C.W., Ashley, M.C.B., Barthelmy, S.D., Flewelling, H.A., Gehrels, N., Göğüş, E., Güver, T., Kiziloğlu, Ü., Krimm, H.A., McKay, T.A., Özel, M., Phillips, A., Quimby, R.M., Rowell, G., Rujopakarn, W., Schaefer, B.E., Smith, D.A., Vestrand, W.T., Wheeler, J.C., Wren, J., Yuan, F., Yost, S.A., 2009. Looking into the fireball: ROTSE-III and Swift observations of early gamma-ray burst afterglows. Astrophys. J. 702, 489–505.

Sakamoto, T., Barthelmy, S.D., Baumgartner, W.H., Cummings, J.R., Fenimore, E.E., Gehrels, N., Krimm, H.A., Markwardt, C.B., Palmer, D.M., Parsons, A.M., Sato, G., Stamatikos, M., Tueller, J., Ukwatta, T.N., Zhang, B., 2011. The second Swift burst alert telescope gamma-ray burst catalog. Astrophys. J. Suppl. Ser. 195, 2.

Sakamoto, T., Lamb, D.Q., Kawai, N., Yoshida, A., Fenimore, C., Graziani, E.E., Donaghy, T.Q., Matsuoka, M., Ricker, M., Suzuki, G., Atteia, J.-L., Shirasaki, Y., Torii, T., Tamagawa, K., Nakagawa, Y., Galassi, M., Doty, J., Crew, R., Vanderspek, G.B., Villasenor, J., Butler, N., Barraud, J.G., Jernigan, C., Bore, M., Dezalay, J.-P., Olive, J.-F., Woosley, S., Hurley, S.E., Pizzichini, G., Hete-2 Science Team, 2005. Global characteristics of X-ray flashes and X-ray rich GRBs observed by HETE-2. Nuovo Cimento C Geophys. Space Phys. C 28, 339.

Sang, Y., Lin, H.-N., Chang, Z., 2016. Testing Einstein's equivalence principle with short gamma-ray bursts: Table 1. Mon. Not. R. Astron. Soc. 460, 2282–2285.

Siellez, K., Boer, M., Gendre, B., Regimbau, T., 2016. Evidence for a dual population of neutron star mergers from short Gamma-Ray Burst observations. ArXiv e-prints.

Song, C.-Y., Liu, T., Gu, W.-M., Tian, J.-X., 2016. Testing black hole neutrino-dominated accretion discs for long-duration gamma-ray bursts. Mon. Not. R. Astron. Soc. 458, 1921–1926.

Troja, E., King, A.R., O'Brien, P.T., Lyons, N., Cusumano, G., 2008. Different progenitors of short hard gamma-ray bursts. Mon. Not. R. Astron. Soc. 385, L10–L14.

Tunnicliffe, R.L., Levan, A.J., Tanvir, N.R., Rowlinson, A., Perley, D.A., Bloom, J.S., Cenko, S.B., O'Brien, P.T., Cobb, B.E., Wiersema, K., Malesani, D., de Ugarte Postigo, A., Hjorth, J., Fynbo, J.P.U., Jakobsson, P., 2014. On the nature of the 'hostless' short GRBs. Mon. Not. R. Astron. Soc. 437, 1495–1510.

Turpin, D., Heussaff, V., Dezalay, J.-P., Atteia, J.-L., Klotz, A., Dornic, D., 2016. Investigating the impact of optical selection effects on observed rest-frame prompt GRB properties. Astrophys. J. 831, 28.

Ukwatta, T.N., Stamatikos, M., Dhuga, K.S., Sakamoto, T., Barthelmy, S.D., Eskandarian, A., Gehrels, N., Maximon, L.C., Norris, J.P., Parke, W.C., 2010. Spectral lags and the lag-luminosity relation: an investigation with Swift BAT gamma-ray bursts. Astrophys. J. 711, 1073–1086.

Virgili, F.J., Qin, Y., Zhang, B., Liang, E., 2012. Spectral and temporal analysis of the joint Swift/BAT-Fermi/GBM GRB sample. Mon. Not. R. Astron. Soc. 424, 2821–2831.

von Kienlin, A., Meegan, C.A., Paciesas, W.S., Bhat, P.N., Bissaldi, E., Briggs, M.S., Burgess, J.M., Byrne, D., Chaplin, V., Cleveland, W., Connaughton, V., Collazzi, A.C., Fitzpatrick, G., Foley, S., Gibby, M., Giles, M., Goldstein, A., Greiner, J., Gruber, D., Guiriec, S., van der Horst, A.J., Kouveliotou, C., Layden, E., McBreen, S., McGlynn, S., Pelassa, V., Preece, R.D., Rau, A., Tierney, D., Wilson-Hodge, C.A., Xiong, S., Younes, G., Yu, H.-F., 2014. The second Fermi GBM gamma-ray burst catalog: the first four years. Astrophys. J. Suppl. Ser. 211, 13.

Wang, F.Y., Dai, Z.G., 2014. Long GRBs are metallicity-biased tracers of star formation: evidence from host galaxies and redshift distribution. Astrophys. J. Suppl. Ser. 213, 15.

Wang, J.S., Wang, F.Y., Cheng, K.S., Dai, Z.G., 2016. Measuring dark energy with the E_{iso}-E_p correlation of gamma-ray bursts using model-independent methods. Astron. Astrophys. 585, A68.

Wei, J.-J., Wu, X.-F., Melia, F., Wei, D.-M., Feng, L.-L., 2014. Cosmological tests using gamma-ray bursts, the star formation rate and possible abundance evolution. Mon. Not. R. Astron. Soc. 439, 3329–3341.

Yonetoku, D., Murakami, T., Tsutsui, R., Nakamura, T., Morihara, Y., Takahashi, K., 2010. Possible origins of dispersion of the peak energy-brightness correlations of gamma-ray bursts. Publ. Astron. Soc. Jpn. 62, 1495–1507.

Zhang, B., Zhang, B.-B., Virgili, F.J., Liang, E.-W., Kann, D.A., Wu, X.-F., Proga, D., Lv, H.-J., Toma, K., Mészáros, P., Burrows, D.N., Roming, P.W.A., Gehrels, N., 2009. Discerning the physical origins of cosmological gamma-ray bursts based on multiple observational criteria: the cases of z = 6.7 GRB 080913, z = 8.2 GRB 090423, and some short/hard GRBs. Astrophys. J. 703, 1696–1724.

Zhang, B.-B., Zhang, B., Sun, H., Lei, W.-H., Gao, H., Li, Y., Shao, L., Zhao, Y., Hu, Y.-D., Lü, H.-J., Wu, X.-F., Fan, X.-L., Wang, G., Castro-Tirado, A.J., Zhang, S., Yu, B.-Y., Cao, Y.-Y., Liang, E.-W., 2017a. A peculiar low-luminosity short gamma-ray burst from a double neutron star merger progenitor. ArXiv e-prints.

Zhang, S., Jin, Z.-P., Zhang, F.-W., Li, X., Fan, Y.-Z., Wei, D.-M., 2017b. Possible correlations between the emission properties of SGRBs and their offsets from the host galaxies. Astrophys. J. 844, 55.

Zou, Y.-C., Wang, F.-F., Moharana, R., Liao, B., Chen, W., Wu, Q., Lei, W.-H., Wang, F.-Y., 2018. Determining the lorentz factor and viewing angle of GRB 170817A. Astrophys. J. 852, L1.